ACS Catalysis

Review

Cite This: ACS Catal. 2018, 8, 6665−6690

pubs.acs.org/acscatalysis

# Electrocatalysts for Hydrogen Oxidation Reaction in Alkaline Electrolytes

Elena S. Davydova,*[,†] Sanjeev Mukerjee,[‡] Frédéric Jaouen,[§] and Dario R. Dekel*[,†]

[†]The Wolfson Department of Chemical Engineering and the Nancy & Stephan Grand Technion Energy Program (GTEP), Technion − Israel Institute of Technology, Haifa 3200003, Israel

[‡]Department of Chemistry and Chemical Biology, Northeastern University, Boston, Massachusetts 02115, United States

[§]Institut Charles Gerhardt Montpellier, UMR 5253, CNRS, Université Montpellier, ENSCM, 34095 Montpellier, France

Supporting Information

**ABSTRACT:** In the past 5 years, advances in anion-conductive membranes have opened the door for the development of advanced anion-exchange membrane fuel cells (AEMFCs) as the next generation of affordable fuel cells. Several recent works have shown that AEMFCs currently achieve nearly identical beginning-of-life performance as state-of-the-art proton exchange membrane fuel cells. However, until now, these high AEMFC performances have been reached with platinum-group metal (PGM)-based anode and cathode catalysts. In order to fulfill the potential of AEMFCs, such catalysts should in the near future be free of PGMs and, eventually, free of critical raw materials. Although great progress has been achieved in the development of PGM-free catalysts for the oxygen reduction reaction in basic media, significantly less attention has been paid to the catalysis of the hydrogen oxidation reaction (HOR). The much lower HOR activity of Pt in basic media compared with that in acid was itself revealed only relatively recently. While several PGM-based composite materials have shown improved HOR activity in basic media, the HOR kinetics remains slower than necessary for an ideal nonpolarizable electrode. In addition, attempts to move away from PGMs have hitherto resulted in high anode overpotentials, significantly reducing the performance of PGM-free AEMFCs. This would be a major barrier for the large-scale deployment of this technology once the other technological hurdles (e.g., membrane stability) have been overcome. A fundamental understanding of the HOR mechanism in basic media and of the main energy barriers needs to be firmly established to overcome this challenge. This review presents the current understanding of the HOR electrocatalysis in basic media and critically discusses the most recent material approaches. Promising future research directions in the development of the HOR electrocatalysts for alkaline electrolytes are also outlined.

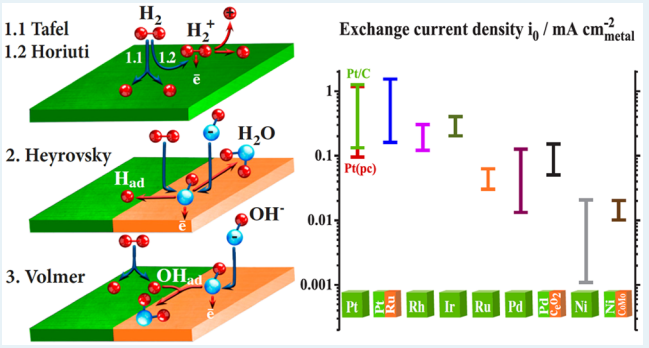


**KEYWORDS:** *hydrogen oxidation reaction, anion exchange membrane fuel cell, alkaline media, electrocatalyst, platinum-group metal, non-noble*



## 1. INTRODUCTION

Anion-exchange membrane fuel cells (AEMFCs) have received increasing attention for more than a decade, mainly because of their potential for resorting to electrocatalysts that are free of platinum-group metals (PGMs) and, eventually, free of critical raw materials (CRMs).[1,2] Recent achievements in developing anion-exchange membranes (AEMs) with high hydroxyl ion conductivity have allowed the fabrication of $H_2$-fed AEMFCs reaching impressive peak power densities of 1.8 and 0.5 W $cm^{-2}$ with cathodes fed with oxygen and air, respectively.[3] However, these recent high beginning-of-life (BoL) performances have been obtained with PGM-based catalysts at both electrodes, usually with Pt/C at the cathode and Pt or a Pt/Ru alloy at the anode.[4−11]

In an effort to logically organize and summarize the BoL performance achieved in previously reported studies, we consider three cases toward PGM-free or Pt-free AEMFCs. In the first case, we consider studies with PGM-based anodes and PGM-free cathodes. The power density spans between 50 and 1500 mW $cm^{-2}$,[12−18] with the BoL performance highly impacted by the oxygen reduction reaction (ORR) activity at the cathode. In the second case, we consider studies with PGM-free anodes and cathodes. In this case, the BoL power density spans between 40 and 120 mW $cm^{-2}$ only,[19−21] as it is strongly limited by the very low hydrogen oxidation reaction (HOR) activity of PGM-free catalysts to date. As a third case, we consider Pt-free AEMFCs with a Pd-based catalyst at either the anode[18,22,23] or the cathode[24,25] in combination with a non-

Received: February 19, 2018
Revised: May 3, 2018
Published: May 31, 2018




DOI: 10.1021/acscatal.8b00689
ACS Catal. 2018, 8, 6665−6690

PGM catalyst at the opposite electrode. In this case, power densities of up to 500 mW $cm^{-2}$ have been achieved.[22] These data show that while alternatives to PGMs already exist for AEMFC cathodes (case 1), no competitive PGM-free catalyst is available today for AEMFC anodes (cases 2 and 3).

This status can be explained historically, with the quest for PGM-free electrocatalysts for the ORR in acidic media having greatly helped in developing metal−N−C catalysts for the ORR in basic media as well.[26−30] The ORR activity of some pyrolyzed Fe−N−C catalysts is now in fact comparable to, or even higher than, that of Pt-based catalysts in basic media. While the definition of surface-specific activity does not apply to Fe−N−C catalysts, it is possible to compare Fe−N−C and Pt/C on the basis of volume-specific activity.[31] In contrast, no such transfer of knowledge has been possible for the HOR from acidic to basic media. No PGM-free catalyst has demonstrated reasonable HOR activity in acidic media to date. Attempts to develop such catalysts have been very scarce because of the very fast HOR kinetics on Pt in acidic media, implying that anodes in proton-exchange membrane fuel cells (PEMFCs) require only an ultralow Pt loading to operate efficiently. The main advantage of AEMFCs versus PEMFCs, i.e. resorting to PGM- and CRM-free catalysts, is thus impaired at this moment by the low HOR activity of PGM-free catalysts in basic media.

To illustrate this better, Figure 1 shows calculated polarization curves for the anode and cathode in an AEMFC,

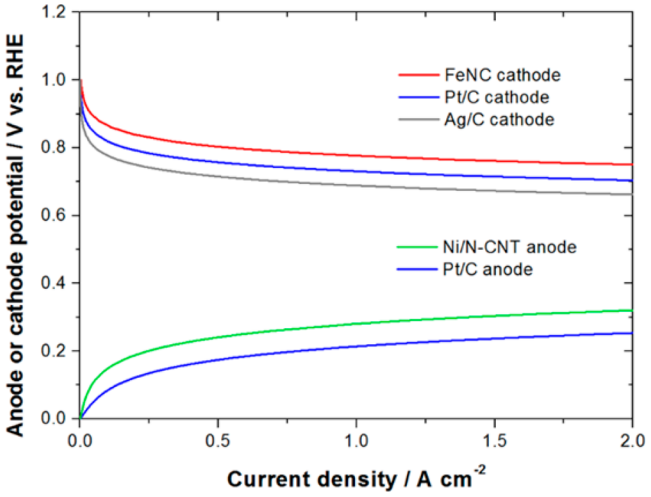


**Figure 1.** Polarization curves for the HOR and ORR calculated using the Butler−Volmer equation for the HOR with exchange current density ($i_0$) and the Tafel equation for the ORR with mass activity or surface-specific activity at 0.9 V vs RHE ($i_{m,\ 0.9\ V}$ or $i_{s,\ 0.9\ V}$, respectively), mimicking the best-in-class PGM-based and PGM-free catalysts.

representing best-in-class PGM-based and PGM-free catalysts. The main assumptions made for the calculations include the Tafel law for the ORR and the Butler−Volmer equation for the HOR, a fuel cell temperature of 60 °C, and an AEM characterized by pH 13. For the cathode catalysts, the following were assumed:

(a) the 40% Pt/C catalyst with the surface area of 50 $m_{Pt}^2$ $g_{Pt}^{-1}$ and $i_{s,\ 0.9\ V} = 10^{-4}$ A $cm^{-2}_{Pt}$,[31,32] the Tafel slope of 90 mV $decade^{-1}$,[33] and the catalyst loading of 600 $\mu$g $cm^{-2}$ (mass of Pt and C). The ORR specific activity at 0.9 V ($i_{s,\ 0.9\ V}$) of Pt nanoparticles in the AEMFC environment at 60 °C was assumed to be $10^{-4}$ A $cm^{-2}_{Pt}$, i.e., ca. 2 times lower than the specific activity of Pt nanoparticles at 0.9 V when measured under PEMFC conditions at 80 °C (about $2 \times 10^{-4}$ A $cm^{-2}_{Pt}$).[32] This assumption is in agreement with the slightly lower ORR activity on Pt single crystals in alkaline versus acidic media.[32] These assumptions result in the mass activity at 0.9 V of 50 A $g_{Pt}^{-1}$, in line with experimentally reported values in 0.1 M KOH.[33]

(b) the Fe−N−C catalyst with the mass activity at 0.9 V of 10 A $g^{-1}$ (per total mass of catalyst).[33] The Fe−N−C cathode loading was assumed to be 2 mg $cm^{-2}$ (mostly carbon, leading to a ca. 50 $\mu$m thick cathode layer), which is on the lower end of the range of non-PGM cathode loadings but leads to a sufficiently thin cathode layer for proper operation with air. The apparent resulting activity of such a Fe−N−C cathode is thus $2 \times 10^{-2}$ A $cm^{-2}_{geom}$ at 0.9 V. The Tafel slope was also assumed to be 90 mV $decade^{-1}$ (as for Pt/C, for fair comparison).

(c) the 40% Ag/C catalyst with the specific surface area of 50 $m^2$ $g_{Ag}^{-1}$ and $i_{s,\ 0.9\ V} = 10^{-5}$ A $cm^{-2}$ (based on the above assumed specific activity for Pt and the one-order-of-magnitude lower surface-specific activity for Ag vs Pt[34]) and the catalyst loading of 2 mg $cm^{-2}$ (mass of Ag and C). The Tafel slope was also assumed to be 90 mV $decade^{-1}$ (as for Pt/C, for fair comparison).

While not represented in Figure 1, pure Mn oxide and bimetallic MnCo oxides have also shown high ORR activity in alkaline media, especially for nanostructured oxide particles with high surface area. From an analysis of selected literature and with an oxide content of 30−50 wt % on carbon for an optimized fuel cell catalyst, the ORR activity at 0.9 V was estimated to range from ca. 1 to 10 A $g_{cat}^{-1}$ for this class of cathode material.[35−37] For a total cathode loading of 2 mg $cm^{-2}$ and a Tafel slope of 90 mV $decade^{-1}$, the resulting calculated polarization curves would range from slightly below the Ag/C one in Figure 1 up to the exact same curve as calculated for the Fe−N−C one in Figure 1.

For the anode catalysts, the following were assumed:

(a) the 40% Pt/C catalyst with the specific surface area of 50 $m_{Pt}^2$ $g_{Pt}^{-1}$ and the exchange current density ($i_0$) of 0.6 mA $cm^{-2}$,[38−41] the catalyst loading of 200 $\mu$g $cm^{-2}$ (mass of Pt and C), and the exchange transfer coefficient of 0.5 (for both the anodic and cathodic directions).

(b) the Ni/N-doped carbon nanotube (Ni/N-CNT) catalyst with $i_0$ = 0.03 mA $cm^{-2}$,[42] the surface area of 25 $m^2$ $g^{-1}$, a catalyst loading of 1 mg $cm^{-2}_{geom}$, and the exchange transfer coefficient of 0.5 (for both the anodic and cathodic directions).

The simulations of anode performance based on electrokinetic losses only (Figure 1) illustrate that the slow HOR kinetics is projected to cause significant voltage loss for the AEMFC at high current density. These calculations are consistent with the experimental AEMFC data reported in the literature. For example, Sheng et al.[38] reported an anode overpotential ($\eta$) of >130 mV at the anode loading of 50 $\mu g_{Pt}$ $cm^{-2}$ and 1.5 A $cm^{-2}$. In addition, Figure 1 shows that even with a Pt/C anode and a significant Pt loading of 0.08 $mg_{Pt}$ $cm^{-2}$, the anode overpotential at 1 A $cm^{-2}$ is projected to be non-negligible. This is in contrast to the case of PEMFCs, where the anode behaves almost as a nonpolarizable electrode.



DOI: 10.1021/acscatal.8b00689
ACS Catal. 2018, 8, 6665−6690

This difference is fundamentally explained by the 2 orders of magnitude lower HOR activity on Pt (and other PGMs) in basic media compared with that in acidic media (Figure 2).

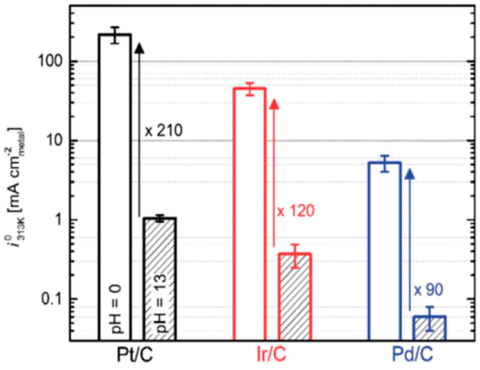


**Figure 2.** HER/HOR exchange current densities measured in 0.1 M NaOH aqueous electrolyte. Data were recorded in a $H_2$-saturated electrolyte at ambient pressure and 40 °C. Reprinted with permission from ref 45. Copyright 2014 Royal Society of Chemistry.

While no PGM-free catalyst has shown decent HOR activity in acidic media to date, slower kinetics toward the hydrogen evolution reaction (HER) in basic versus acidic media has also been reported for PGM-free catalysts,[43,44] possibly supporting a universal effect of pH on the rates of the HER and HOR. In summary, resorting to ultralow or even zero PGM content at the anode of an AEMFC with present PGM- or non-PGM catalysts leads to an unacceptably high anode overpotential. Novel materials must be designed whose intrinsic HOR activity is higher than presently reached with existing materials and whose surface is not blocked for the HOR catalysis by the formation of oxide at low overpotential.

In order to help foster rational approaches for the development of highly active PGM-based and PGM-free catalysts, this review covers a series of aspects of the HOR electrocatalysis, including the hypothesized HOR mechanisms in basic media and the effects of electrocatalyst affinity toward hydrogen or hydroxyl chemisorption on the HOR kinetics. The already developed mono- or bifunctional HOR electrocatalysts are reviewed in the light of this understanding and are classified according to the mechanisms by which they catalyze the HOR.

## 2. ROTATING DISK ELECTRODE AND ALTERNATIVE METHODS TO MEASURE THE HOR ACTIVITY

The rotating disc electrode (RDE) technique is the most common experimental technique applied for the HOR kinetic studies in liquid electrolytes.[38,46,47] Applying the well-known Levich and Koutecky–Levich equations, one can correct the measured $I$ versus $E$ polarization curves for (i) Ohmic drop in the electrolyte (typically 10–20 Ω in RDE setups depending on the nature and concentration of the electrolyte, resulting in a maximum Ohmic drop of ca. 10 mV at the diffusion-limited current density for an RDE tip geometric area of 0.2 $cm^2$) and (ii) the $H_2$ diffusion limitation and extract the kinetic current density values (polarization overpotential). One general precaution to recall when applying the RDE to the HOR reaction (a sometimes quasi-reversible reaction, depending on the catalyst and electrolyte pH) is the impossibility of assessing the HOR activity for catalysts whose exchange current density is commensurate with or higher than the diffusion-limited current density, $i_{lim}$. For example, as a result of high $i_0$ values on Pt in acidic electrolytes, the reaction rate in the RDE becomes limited by hydrogen diffusion in the electrolyte toward the electrode, even at very low overpotentials. The measured polarization curve (see Figure 3A, curve labeled $\eta_{diffusion}$) then

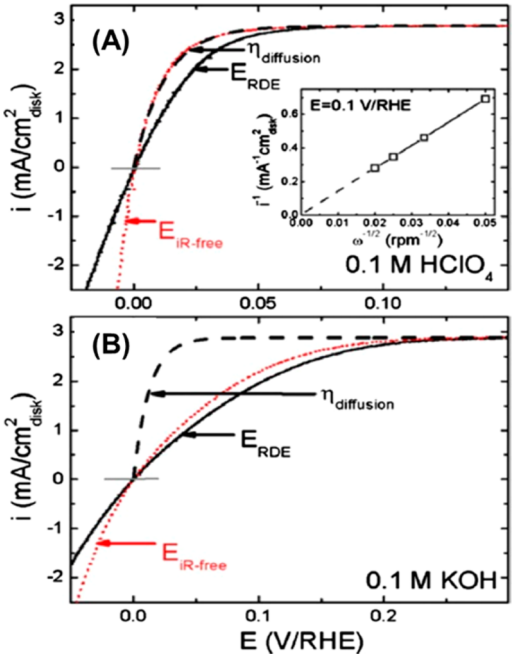


**Figure 3.** (A) HOR/HER polarization curves on polycrystalline platinum (Pt(pc)) in 0.1 M $HClO_4$ at 1600 rpm, as measured (solid black line, $E_{RDE}$) and after Ohmic drop correction (dotted red line, $E_{iR\text{-free}}$). The dashed black curve labeled $\eta_{diffusion}$ represents the theoretical curve for which there is no kinetic polarization of the electrode, only $H_2$ concentration polarization. The inset shows the Koutecky–Levich plot obtained at $E$ = 0.1 V vs RHE for the HOR at different rotation rates. (B) HOR/HER polarization curves on Pt(pc) in 0.1 M KOH at 1600 rpm. Reprinted with permission from ref 38. Copyright 2010 The Electrochemical Society.

only reflects a hydrogen concentration polarization that is not related to the kinetics (eq 1):

$$\eta_{diffusion} = \frac{RT}{2F} \ln\left(1 - \frac{i}{i_{lim}}\right) \quad (1)$$

Thus, quantification of the HOR kinetics by the RDE method is difficult for very active catalysts.[38] This was explained only recently to lead to a broad range of experimentally reported values in acidic electrolytes.[48,49] This limitation of the RDE method is currently less important for PGM-based and even more so for non-PGM-based HOR catalysts in alkaline media because of their lower activity. This is shown in Figure 3B from the large positive shift of the experimentally measured RDE polarization curves relative to the theoretical curve expected for $H_2$ concentration polarization only (eq 1).

In the future, for highly active HOR catalysts in alkaline electrolytes with $i_0$ values too high to be measured with the RDE technique, transient techniques such as rapid potentiodynamic scanning[50,51] or other steady-state methods that allow higher mass transport (microelectrodes) may be used.[48] For the HOR kinetics evaluation on powder catalysts, the cavity microelectrode technique, which was developed for both liquid[52] and solid electrolyte conditions,[53,54] is also applicable.


DOI: 10.1021/acscatal.8b00689
ACS Catal. 2018, 8, 6665–6690

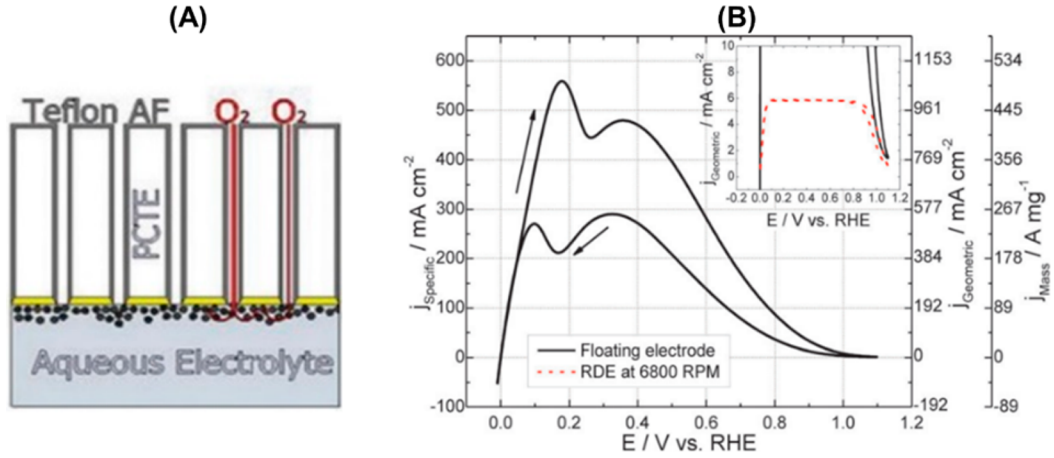


**Figure 4.** (A) Structure of the working electrode, made up of catalyst deposited onto a gold-coated porous polycarbonate track-etch membrane. The pores are coated with the hydrophobic amorphous fluoropolymer to keep the pores open for reactant gas (in this case oxygen) to flow to the catalyst from behind. (B) Comparison of the HOR polarization curves measured by the floating electrode and RDE methods using 2.2 $\mu g_{Pt}$ $cm^{-2}$ Pt/C catalyst at 10 mV $s^{-1}$ at 298 K. Reprinted with permission from ref 55. Copyright 2013 The PCCP Owner Societies.

As an alternative to the RDE method, the floating electrode technique was proposed by Zalitis et al.[55] in order to investigate the HOR electrocatalysts. It combines the high mass transport rate characteristic of gas-diffusion electrodes in fuel cells with a flat, uniform, and homogeneous catalyst deposition process. This approach closely mimicks the operating conditions of AEMFCs or PEMFCs (gas-fed electrodes). Uniform Pt layers were produced with loadings down to 0.16 $\mu g_{Pt}$ $cm^{-2}$ and a thickness of 200 nm on polycarbonate track-etch membrane filter/Au floating electrodes (Figure 4). The HOR revealed fine structure in the diffusion-limited current range and an asymptotic current decay for potentials above 0.36 V due to the formation of oxides on the platinum surface and adsorption of anions, which are not visible with techniques limited by mass transport in aqueous media such as the RDE method.

Kinetic data on the HOR have also been obtained in single-cell fuel cell applying the electrochemical hydrogen pumping mode (Figure 5).[56] In these systems, hydrogen oxidation occurs at the anode (working electrode) and hydrogen evolution at the cathode, with protons or hydroxyl ions transferred via the proton-exchange membrane (PEM) or AEM, respectively. In order to study the HOR kinetics, the anode is coated with the HOR catalyst under investigation (for PGM-based catalyst, at an ultralow loading, e.g., 3 $\mu g_{Pt}$ $cm^{-2}$) while the cathode is coated with high loading of Pt/C (e.g., 0.4 $mg_{Pt}$ $cm^{-2}$), de facto acting as a reference electrode.[57] By the use of this $H_2$ pump method with an AEM, the $i_0$ value of the HOR on Pt/C interfaced with an anion-exchange ionomer (AEI) was reported for the first time.[58] It was found that the HOR activity at the Pt/C−AEI (Tokuyama A201) interface is almost the same as in 0.1 M KOH, both activities being nearly 2 orders of magnitude lower than that measured in acidic electrolytes, either the PEM electrolyte (Nafion 211) or 0.1 M $HClO_4$.

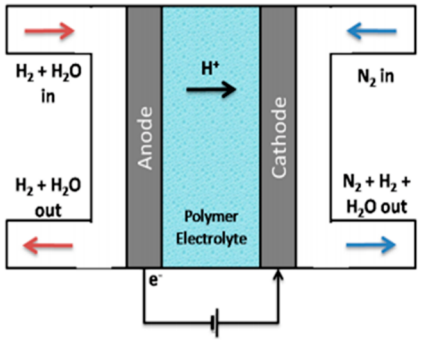


**Figure 5.** Representation of a PEM device operating in hydrogen pumping mode. Humidified hydrogen is fed at the anode, and dry nitrogen is fed at the cathode. The hydrogen molecule dissociates into protons and electrons at the anode, and the latter recombine into $H_2$ at the cathode.

## 3. GENERAL PRINCIPLES OF THE HOR IN BASIC MEDIA

**3.1. Pathway of the HOR in Alkaline Media.** It is widely agreed, at least for inorganic materials, that the HOR in alkaline media proceeds through a combination of the following elementary steps: (A) dissociative adsorption of molecular dihydrogen, (B) electron transfer from molecular dihydrogen to the catalyst, and (C) discharge of the adsorbed hydrogen atom. Hereafter we describe these three steps.

(A) Dissociative adsorption of molecular dihydrogen, $H_2$, without electron transfer, which is known as the Tafel (*T*) reaction[59] (eq 2):

$$H_2 + 2^* \rightarrow 2(^*{-}H_{ad}) \quad (2)$$

where $H_2$ is molecular dihydrogen in the vicinity of the catalyst surface, * is an active site, and $H_{ad}$ is a chemisorbed hydrogen atom (or adatom). The dissociation energy of the $H_2$ molecule is 4.52 eV at a separation of 0.74 Å.[60] One of the requirements imposed on the catalytic materials is affinity toward molecular hydrogen chemisorption. Therefore, the $^*{-}H_{ad}$ binding energy is believed to be a crucial factor controlling the HOR kinetics.[39,61] The surface intermediate of adsorbed hydrogen on Pt microelectrodes was shown to be independent of solution pH.[62] Also, as was revealed previously for chalcogenides ($RuS_2$, Co-doped $RuS_2$),[63] the ability to dissociate $H_2$ at room temperature is a necessary but not sufficient criterion for the HOR catalyst.

The dissociative adsorption of the diatomic molecule $H_2$, a central step in many industrially important catalytic processes, is generally assumed to require at least two adjacent and empty atomic adsorption sites (or vacancies).[64] The need for


DOI: 10.1021/acscatal.8b00689
ACS Catal. 2018, 8, 6665−6690

ensembles of PGM atoms is experimentally supported by the lack of the HOR activity of Pt atoms atomically dispersed as $PtS_4$ moieties on a sulfur-doped carbon matrix.[65] $H_2$ is known to be a chemically reactive gas, which adsorbs dissociatively on most transition metal surfaces with heats of chemisorption between 60 and 120 kJ $mol^{-1}$. For example, according to the linear dependence $\theta_H - p_{H_2}^{0.5}$,[64] hydrogen is considered to adsorb in the atomic state.

According to Christmann,[66] the preferential adsorption site has high coordination. Threefold sites are favored on diagonal, trigonal, and hexagonal surfaces, while fourfold sites are the rule for tetragonal surfaces. The latter should therefore adsorb $H_2$ more strongly for a given metal. There is ample evidence that strong chemisorption of a hydrogen atom requires three to seven adjacent metal atoms, coined as the ensemble effect.[67] Mitsui et al.[68] have shown that the creation of active sites for $H_2$ dissociation involves the formation of individual vacancies and their subsequent diffusion and aggregation, with the coupling between these events determining the activity of the catalyst surface. Their scanning tunneling microscopy observations of the transient formation of active sites for the dissociative adsorption of $H_2$ molecules on Pd(111) revealed that two-vacancy sites are inactive. Two-vacancy sites have low $H_2$ sticking probability and zero $H_2$ adsorption events (Table 1).

**Table 1. Active-Site Statistics for Vacancy Clusters for Pd(111) at 65 K in $2 \times 10^{-7}$ Torr $H_2$ As Determined by Scanning Tunneling Microscopy with a Frame Time of 75 s[68]**

| vacancy cluster size (atoms) | 2 | 3 | 4 | 5 |
|---|---|---|---|---|
| mean adsorption time (s) | $>2 \times 10^4$ | 330 | 150 | 120 |
| $H_2$ sticking coefficient | <0.0001 | 0.005 | 0.008 | 0.008 |
| mean cluster separation time (s) | 590 | 710 | 670 | 820 |

Aggregates of three or more hydrogen vacancies are therefore required for efficient $H_2$ dissociation. At higher coverages of $H_{ad}$, indirect interactions come into play, which are in most cases repulsive. They lead to a substantial lowering of the initial metal–hydrogen binding energy (HBE), a phenomenon called induced surface heterogeneity. Consequently, weakly held (and chemically reactive) hydrogen species are formed. The observations made by the authors[68] might be used as an approach to synthesize new electrocatalytic materials with a controlled number of adjacent active sites (having initially high HBE) "diluted" by inactive atoms in order to tune the HBE.

(B) Electron transfer from molecular dihydrogen to the catalyst, which is known as the Heyrovsky (***H***) reaction[69] (eq 3):

$$H_2 + OH^- + * \rightarrow (*{-}H_{ad}) + H_2O + e^- \quad (3)$$

where $OH^-$ is in the vicinity of the catalyst surface. The species is argued not to be $OH^-$ but most likely $OH_{ad}$.[18,22,70] If this is the case, the ***H*** reaction could be written as eq 4:

$$H_2 + (*{-}OH_{ad}) \rightleftarrows (*{-}H_{ad}) + H_2O \quad (4)$$

with the assumption that the reaction is preceded by hydroxide adsorption (eq 5):

$$OH^- + * \rightleftarrows (*{-}OH_{ad}) + e^- \quad (5)$$

Thus, it is supposed that the catalyst surface should be oxophilic, or "hydroxophilic", in order to provide bifunctional catalysis (Figure 6),[22,70,71] which will be discussed in section 4.2. In alkaline media, the catalytic surface has to provide active sites for the coadsorption of hydrogen atoms and hydroxide species, whereas in acid all of the accessible active sites are destined to uniquely chemisorb hydrogen atoms. This could explain, among other reasons, why catalysts exhibit several times to several orders of magnitude lower electrochemical HOR activity in alkaline environments compared with acidic environments (Figure 2).[38,39,45,58]

(C) Discharge of the adsorbed hydrogen atom ($H_{ad}$), which is called the Volmer (***V***) reaction[72] (eq 6):

$$(*{-}H_{ad}) + OH^- \rightarrow * + H_2O + e^- \quad (6)$$

Nondissociative adsorption of hydrogen to form a hydrogen molecule ion intermediate was also proposed by Horiuti[73,74] as the rate-determining step (RDS) for some substrates according to the following reactions (eqs 7 and 8):

$$H_2 + * \rightleftarrows H_2M \rightarrow H_2^+M + e^- \quad (7)$$

$$H_2^+M \rightleftarrows MH + H^+ \quad (8)$$

The essential feature of the Horiuti mechanism is that the hydrogen molecule adsorption step is not accompanied by hydrogen dissociation and requires only a single-atom catalyst for the reaction. In the Heyrovsky–Volmer (***H–V***) sequence, hydrogen adsorption is dissociative but requires only a single

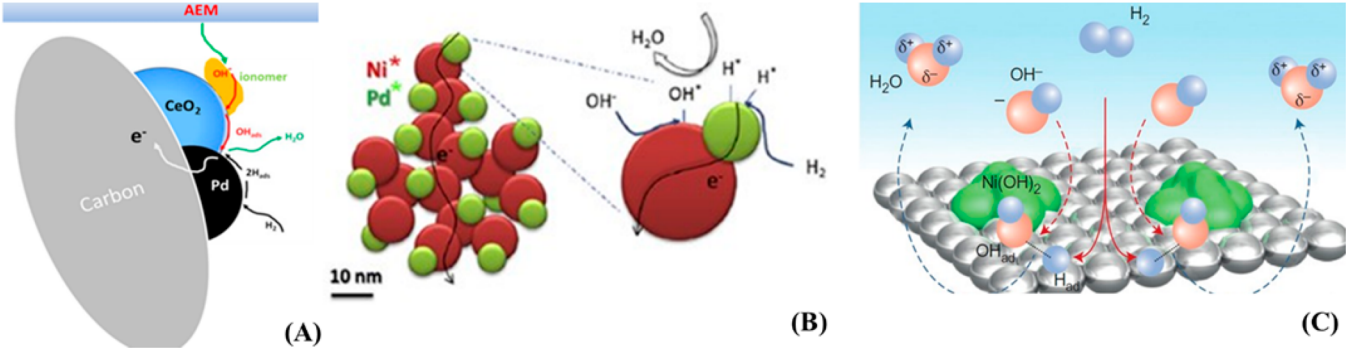


**Figure 6.** Schematic representations of the hypothesized bifunctional mechanism in the HOR electrocatalysis on (A) Pd/C–$CeO_2$, (B) PdNi, and (C) $Ni(OH)_2$/Pt(111). $CeO_2$ in (A), Ni in (B), and $Ni(OH)_2$ in (C) provide the active sites for adsorption of reactive $OH_{ad}$, and Pd (or Pt) provides the active sites for dissociative adsorption of $H_2$ and production of $H_{ad}$, which then reacts with $OH_{ad}$. Reprinted with permission from refs 18 and 70. Copyright 2016 Elsevier and 2013 Springer Nature, respectively.



DOI: 10.1021/acscatal.8b00689
ACS Catal. 2018, 8, 6665–6690

site. Only the Tafel–Volmer (***T*–*V***) sequence requires dual sites, which are nearest-neighbor sites for hydrogen dissociation.

The oxidation rate of preadsorbed hydrogen atoms on Pt was found[75] to be at least an order of magnitude greater than the electrochemical rate of hydrogen molecule oxidation.[76] Although the authors believe that these results exclude the ***V*** reaction from being the RDS,[76] they do not provide differentiation between the ***T*–*V***, ***H*–*V***, and Horiuti (***Ho***) mechanisms. This suggests that such differentiation could be provided by separately measuring the rates of the ***T*** and ***H*** reactions on the Pt surface.

It is possible to measure the rate of gas-phase hydrogen dissociative chemisorption on Pt in the absence of electron transfer. With the hydrogen dissociative step as the RDS, the anodic current density will be given by eq 9:[51]

$$i_a = nFk_a c_{H_2}(1 - \theta) - nFk_c\theta^2 \tag{9}$$

where $\theta$ is the coverage of the metal surface by adsorbed hydrogen and $k_a$ and $k_c$ are the anodic and cathodic rate constants, respectively, analogously to the gas-phase kinetics. Ross and Stonehart[51] proposed that the HOR follows the ***T*–*V*** sequence with the ***T*** reaction as the RDS on Pt. A direct discharge of $H_2$ has also been proposed, with the extraction of two electrons on polycrystalline platinum (Pt(pc)) in 1 M NaOH according to the value of the Tafel slope (70 mV decade$^{-1}$) and the good linear fit of the experimental data to eq 10:[49]

$$\frac{i}{1 + \frac{i}{i_{lim}} - \exp(-2f\eta)} = i_0 \exp(2\alpha f\eta) \tag{10}$$

where $f = RT/F$, $n$ is the number of electrons in the RDS, and $\alpha$ is the charge transfer coefficient of the RDS, leading to the values $i_0$ = 0.233 mA cm$^{-2}{}_{Pt}$, $n$ = 2, and $\alpha$ = 0.43.

The reported data on the HOR kinetics and mechanism for platinum-based electrocatalysts in basic media in the temperature range of 2–70 °C are summarized in Table S2.

This section has summarized the possible HOR mechanisms in alkaline media, considering in detail the Tafel, Heyrovsky, Volmer, and Horiuti mechanisms. Experimental evidence for each mechanism is provided, which reveals, as outlined in Table 2, that the HOR mechanism is still disputable, even for well-studied Pt catalysts. In the next section, more attention is paid to the role of dissociative chemisorption (Tafel reaction) of hydrogen on the kinetics of the HOR.

**3.2. Thermodynamics of Hydrogen Chemisorption and Hydrogen Binding Energy.** Some authors claim[39,45,77] that the HBE is a sufficient descriptor to entirely determine the HOR kinetics. While this may be true for model surfaces of a single metal that are free of topological or chemical heterogeneity, the existence of such a surface under real conditions is highly improbable. Heterogeneities in surfaces or chemical heterogeneities (bimetallic catalysts, etc.) therefore lead to a more complex case. Nevertheless, the HBE descriptor has been found to be a powerful tool to describe the main trends in the HER/HOR reactivity on monometallic catalysts and core–shell catalysts in base (eq 11) and in acid (eq 12):

$$H_2 + 2OH^- \rightleftarrows 2H_2O + 2e^- \tag{11}$$

$$H_2 \rightleftarrows 2H^+ + 2e^- \tag{12}$$

**Table 2. Summary of Probable HOR Mechanisms on Pt-Based Electrocatalysts in Basic Solutions Confirmed Experimentally and Expected Consequences Thereof**

| HOR mechanism | experimental evidence | hypothesized consequences |
|---|---|---|
| dual-site $H_2$ dissociation (Tafel): $H_2 + 2^* \rightarrow 2(^*{-}H_{ad})$ | 1. The HOR rate is close to the $H_2 \leftrightarrow D_2$ exchange rate in the gas phase.[51] | 1. Dual-site adsorption. |
| | 2. The rate of oxidation of preadsorbed $H_{ad}$ is at least an order of magnitude greater than the HOR rate.[76] | 2. No electrolyte effect. |
| | 3. The HOR is size-independent, while oxidation of $^*{-}H_{ad}$ is size-dependent.[38] | 3. No support material effect. |
| | 4. There is a linear correlation between $i$ and $\theta_{H_{UPD}}$[a] with a slope of 2.[46] | 4. No size effect. |
| | 5. $i_0$ is not pH-dependent.[62] | 5. No spillover effect. |
| | | 6. The $^*{-}H_{ad}$ binding energy is the crucial factor controlling the HOR/HER kinetics. |
| dual-site discharge of adsorbed hydrogen atom (Volmer): $(^*{-}H_{ad}) + OH^- \rightarrow {}^* + H_2O + e^-$ | 1. Good fit of the data to the Butler–Volmer equation.[39] | 1. Dual-site adsorption. |
| | 2. There is a correlation between the HOR activity and the HBE derived from the $H_{UPD}$[a] peak potential.[39] | 2. Spillover effect. |
| | 3. Identical activities are determined from the HOR measurements and the $H_{UPD}$ charge transfer resistance.[45] | 3. The $^*{-}H_{ad}$ binding energy is the crucial factor controlling the HOR/HER kinetics. |
| | | 4. $^*{-}OH$ adsorption is the crucial factor controlling the HOR/HER kinetics. |

[a]$H_{UPD}$ denotes underpotential-deposited hydrogen.



DOI: 10.1021/acscatal.8b00689
ACS Catal. 2018, 8, 6665–6690

The HBE has a pure thermodynamic definition, sometimes interpreted as the reaction enthalpy (eq 13 or the simplified form, eq 14) or as the metal−hydrogen binding energy (eq 15):

$$\Delta H_{H_{ad}} = -E_{H_{UPD}}F - TS^{\circ}_{H_2}/2 + gRT \quad (13)$$

where $\Delta H_{H_{ad}}$ is the enthalpy of hydrogen adsorption, $E_{H_{UPD}}$ is the potential (vs the reversible hydrogen electrode (RHE)) of underpotential deposition (UPD) of hydrogen, $S^{\circ}_{H_2}$ is the standard entropy of $H_2$ adsorption (−130.684 J $mol^{-1}$ $K^{-1}$), and $g$ is a dimensionless interaction parameter in the frame of Frumkin adsorption ($g < 0$ for attractive interactions and $g > 0$ for repulsive interactions);[61]

$$\Delta H_{H_{ad}} = -E_{H_{UPD}}F - TS^{\circ}_{H_2}/2 \quad (14)$$

for the Langmuir isotherm of adsorption (with $g = 0$);

$$E_{M-H} = -D_{H_2}/2 - E_{H_{UPD}}F - TS^{\circ}_{H_2}/2 \quad (15)$$

where $E_{M-H}$ is the metal−hydrogen binding energy and $D_{H_2}$ is the dissociation energy of the $H_2$ molecule (432 kJ $mol^{-1}$).[61,78]

Certain formulas can be obtained, for example eqs 16[39] and 17,[79] to estimate the $i_0$ value, which is the kinetic parameter at or near equilibrium conditions (zero overpotential):

$$i_0 = A \exp\left(-\frac{\beta FE_{peak}}{RT}\right) \quad (16)$$

where $E_{peak}$ is the potential of $H_{UPD}$ desorption;[39]

$$i_0 = k_0 \frac{1}{1 + \exp\left(-\frac{\Delta G_{H_{ad}}}{k_B T}\right)} \exp\left(-\frac{\Delta G_{H_{ad}}}{k_B T}\right) \quad (17)$$

where $k_B$ is Boltzmann's constant and $\Delta G_{H_{ad}}$ is the free energy of hydrogen adsorption, which is described by the equation $\Delta G_{H_{ad}}$ = HBE + 0.24 eV. A volcano-type correlation between the HBE values and exchange current densities with the maximum at $\Delta G_{H_{ad}} \sim 0$ eV was observed for the HER and HOR (Figure 7).[79]

The HBE is a thermodynamic parameter that can be employed to predict either the HOR or HER kinetics near equilibrium without distinction on the nature of the electrolyte (acid or basic medium). However, this does not necessarily mean that the HBE values might be used to predict the HOR kinetics far from equilibrium. Moreover, equality of the theoretically predicted exchange current density values for the HOR and HER does not necessarily imply the similarity in the kinetics and mechanism of the reactions. For instance, it is well-known that the HER kinetics on Ni-based electrocatalysts suffers from deactivation via nickel hydride formation,[80] whereas the HOR kinetics is limited by the surface passivation via nickel hydroxide formation.[81] Another example supporting this is given by Vilekar et al.[82] in a theoretical study to explain the strong asymmetry observed in current versus potential curves for the HER and HOR branches on Pt in 0.5 M NaOH. The authors found that the ***H−V*** pathway is dominant in the regions −0.3 to −0.24 and +0.13 to +0.3 V vs RHE, whereas the ***T−V*** mechanism dominates in the regions −0.1 to 0 V and 0 to 20 mV vs RHE.[82]

The majority of HBE values reported in the literature (Table S1) were determined theroretically, with the exception of some studies[39,77,83] where the thermodynamic parameters were

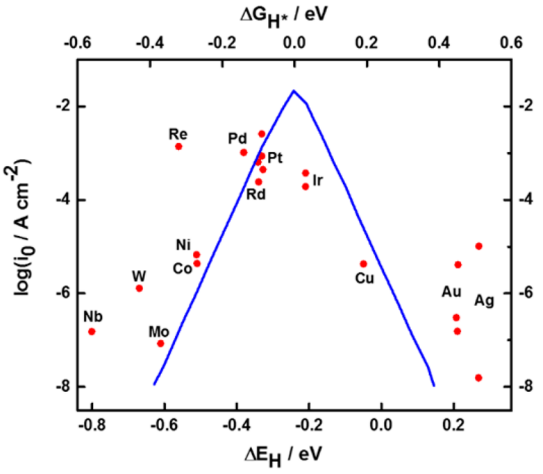


**Figure 7.** Experimentally measured HER/HOR exchange current densities (marked as dots) over different metal surfaces in acid solutions, plotted as a function of the calculated HBE. The solid blue line is the simple kinetic model plotted either as a function of the free energy for hydrogen adsorption according to eq 17 or as a function of HBE. Reprinted with permission from ref 79. Copyright 2005 The Electrochemical Society.

estimated from the $H_{UPD}$ peak potential values given the assumption that $H_{UPD}$ is identical to the HOR intermediate. Though the binding energy values are scattered depending on the type of material (bulk, pc, facet), the nature of the H adsorption site (on top, face-centered cubic (FCC), monolayer (ML), etc.), and the coverage of the suface by $H_{ad}$ ($\theta$), the HBE values are correlated with the atomic numbers of the main components, as illustrated in Figure 8. The main components are represented by 18 different elements of period 4 (Ti, V, Cr, Fe, Co, Ni, and Cu), period 5 (Mo, Ru, Rh, Pd, and Ag), and period 6 (W, Re, Os, Ir, Pt, and Au) that are potentially considered as components of the HOR electrocatalysts because of their high $H_2$ sticking probability (or sticking coefficient, i.e., the ratio of the number of particles being bound to the number hitting the surface).[66]

This section has provided the key equations relating thermodynamic parameters of the hydrogen adsorption/desorption process such as the HBE, metal−hydrogen binding energy, and free energy of hydrogen adsorption. An extensive number of reported HBE values, along with other thermodynamic parameters, both theoretical and experimental, have been summarized for a series of catalysts (elements of periods 4−6), taking into account the type of material, nature of adsorption site, and the coverage of the suface. The HBE values have been, within each given period of elements, successfully correlated with the atomic numbers of the elements, identifying Ni, Pd, and Pt as potentially highly reactive metallic elements for the HER/HOR catalysis within the corresponding transition metal groups. Equations to calculate the values of exchange current density of the HOR, given the Tafel mechanism of the HOR, have also been given in this section. Since HBE is still considered one of the key HOR descriptors, the summarized data may temporarily serve as a useful reference database for future studies.

**3.3. Effect of Underpotential- and Overpotential-Deposited Hydrogen.** The HOR occurs at positive potentials with respect to the RHE. Thus, overpotential-deposited hydrogen ($H_{OPD}$), which is believed to form at negative potentials and to precede the HER[84] (the existence of the



DOI: 10.1021/acscatal.8b00689
ACS Catal. 2018, 8, 6665−6690

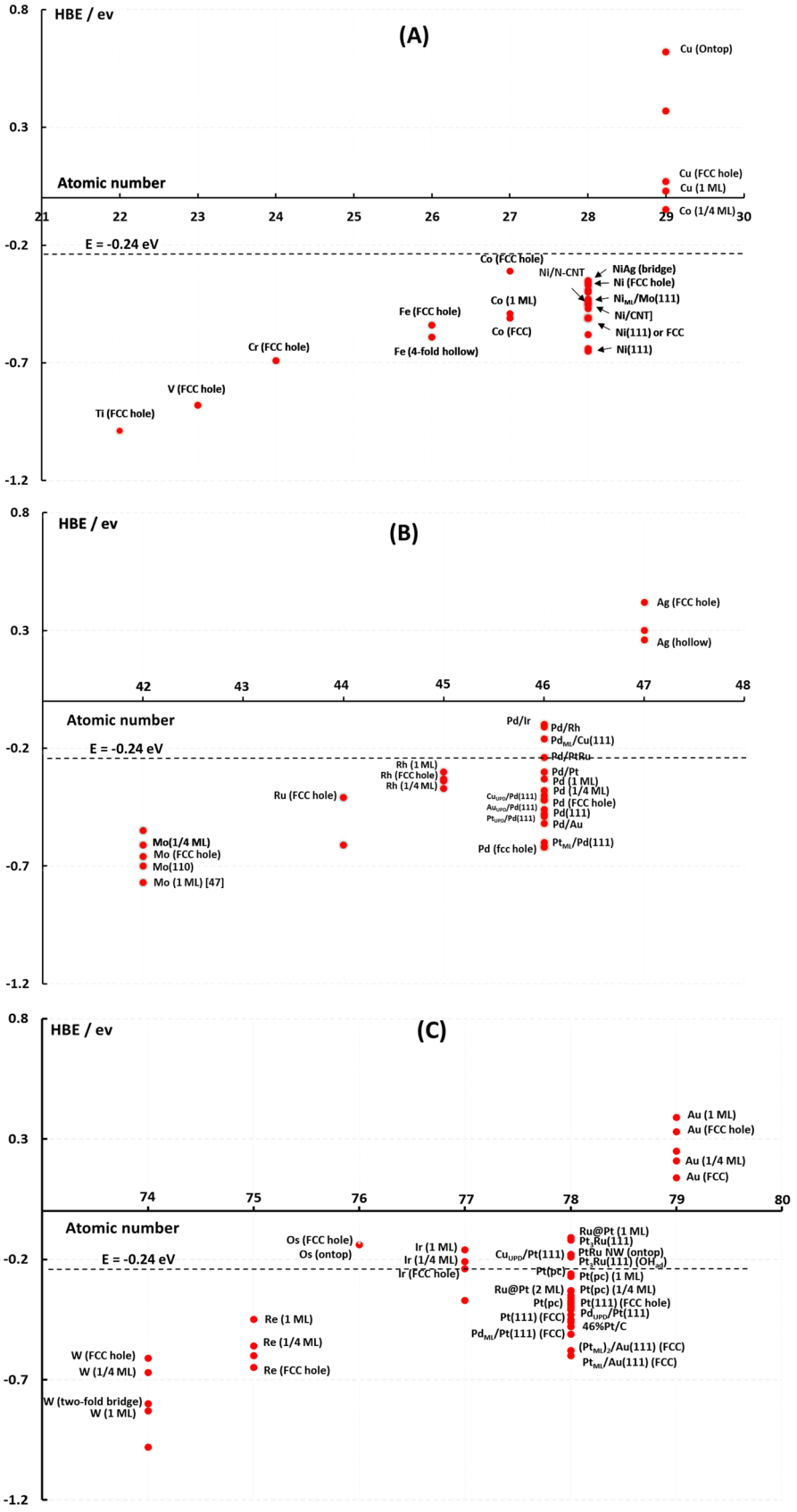


**Figure 8.** Periodic dependence of selected theoretically calculated HBE values for different elements: (A) period 4: Ti, V, Cr, Fe, Co, Ni, and Cu; (B) period 5: Mo, Ru, Rh, Pd, and Ag; (C) period 6: W, Re, Os, Ir, Pt, and Au.

species is disputed in the literature),[45] is out of the scope of the current review. Cyclic voltammetry in the range of potentials more positive than the RHE reveals that not all materials having high $H_2$ sticking probability[66] are able to host the so-called



DOI: 10.1021/acscatal.8b00689
ACS Catal. 2018, 8, 6665−6690

underpotential-deposited hydrogen atoms ($H_{UPD}$). As an example of such materials, we can find Re,[85,86] Ni,[87,88] Fe,[89−91] and Ti−Ni.[92] Thus, $H_{UPD}$ in aqueous solution is a phenomenon characteristic of certain metals,[84] such as Pt,[38] Rh,[93] Pd,[39] Ru,[94] Ir,[61,95] and Mo,[96] both in acidic and basic electrolytes. The origin of hydrogen underpotential deposition is purely thermodynamic; on the other transition metals, $H_{UPD}$ formation does not take place in the same or other potential regions because of the electrosorption of O-containing species, namely, oxygen or hydroxide, which is energetically more favorable. Thus, the effect of $H_{UPD}$ formation can be ruled out in the case of non-PGM catalysts but cannot be straightforwardly excluded for PGMs.

An interesting question concerns the role that $H_{UPD}$ may play in the electrochemical oxidation of hydrogen molecules. It is believed that the electrocatalytic oxidation of hydrogen molecules on Pt essentially involves atomic H in a chemisorbed state, Pt−$H_{ad}$, as a reactive intermediate. There are debates in the literature on the chemical nature of $H_{ad}$,[48,50,84] and currently there are two viewpoints. In one, $H_{UPD}$ is considered as the intermediate involved in the HOR;[84] in the other, it is believed that another form of adsorbed hydrogen acts as the intermediate and $H_{UPD}$ acts as a blocking intermediate.[46,97]

Different isotherms for $H_{UPD}$ and very different reactivity values for the HOR were obtained for Pt(111), Pt(100), and Pt(110) single-crystal surfaces in basic media (Figure 9).[46] The HOR was shown to occur on Pt(110) even on a surface fully covered by $H_{UPD}$. On Pt(100) and Pt(111), the HOR onset appeared to correlate with the desorption of $H_{UPD}$. The Pt(111) surface with $H_{UPD}$ coverage higher than 0.5 ML was shown to be almost completely inactive for the HOR. Kinetic analysis according to the empirical relation between $H_{UPD}$ and the number of bare Pt sites available for $H_2$ dissociation (eq 18),

$$H_{UPD} = i_{\theta_{H_{UPD}=0}} \times (1 - \theta_{H_{UPD}})^m \tag{18}$$

revealed that Pt(111) in alkaline solution follows the ideal dual-site form of the ***T*−*V*** sequence with $m = 2$, whereas the Pt(110) surface does not fit the model in the sense that $m = 0.5$ does not have a physical meaning. Marković et al.[46] hypothesized that there are sites for $H_2$ dissociation on the Pt(110) surface that are not occupied by $H_{UPD}$, although a full monolayer of hydrogen is adsorbed.

Strong inhibition of the HOR in the $H_{UPD}$ potential region was also observed for Pt(111), Pt(100), and Pt(110) single-crystal surfaces in 0.1 M KOH over the temperature range 2−60 °C;[97] however, it was also proposed that $OH_{ad}$ coadsorbs with $H_{UPD}$ on all three surfaces in the $H_{UPD}$ potential region,[98] according to the significant reaction rates of CO oxidation at $E < 0.1$ V. As an indirect proof, the maximum coverage of $H_{UPD}$ before the onset of the HER was determined to be 0.82, 0.78, and 0.65 ML on Pt(110), Pt(100), and Pt(111), respectively (1 ML ≡ 1 $H_{UPD}$ per Pt), the rest likely being covered by $OH_{ad}$. For the HOR, the $H_{UPD}$ reaction can formally be considered as the Volmer reaction, which is the RDS. To support this hypothesis, Durst et al.[45] compared the charge transfer resistance (CTR, $R_{CT}$) for the $H_{UPD}$ reaction with the exchange current density of the HOR/HER, derived from eq 19:

$$i_0 = \frac{RT}{F} \times \frac{i}{\eta} = \frac{RT}{F} \times \frac{1}{R_{CT}} \tag{19}$$

The exchange current density values for the Volmer reaction estimated by Durst et al. are very similar to the HOR exchange current densities of ca. 200 mA $cm^{-2}$ on Pt/C. In 0.05 M NaOH, the charge transfer resistance of 13−54 Ω $cm^{-2}$ obtained on single-crystal Pt surfaces[99] corresponds to 0.2−0.5 mA $cm^{-2}_{Pt}$ which is very close to the value of 1.0 mA $cm^{-2}_{Pt}$ obtained for Pt/C in 0.1 M NaOH. One possibility for the reduced rate of the Volmer step in base would be a higher Pt−H bond strength, which would decrease the HOR rate. A higher Pt−H bond strength is confirmed by the positive shift of the $H_{UPD}$ peaks with respect to the RHE with increasing pH. These shifts on Pt(553) and Pt(533)[100] as well as on Pt(pc),[101] amount to −10 and −11 mV vs RHE per pH unit, respectively (see other values of d(HBE)/d(pH) in Table S2). The $H_{UPD}$ peak shift translated into an HBE difference of 12.5−13.5 kJ $mol^{-1}$ from pH 0 to pH 13. If the difference in the HBE is assumed to be proportional to the difference in the activation energy (according to the Brønsted−Evans−Polanyi relationship),[102] then the difference in the HOR rate between pH 0 and pH 13 for Pt would amount to a factor of 120−200. This difference is in good agreement with the 210-fold difference in $i_{0,\ 313\ K}$ values at pH 0 and pH 13 (see Figure 2),[45] strengthening the hypothesis that the Volmer step is the RDS for the HOR on Pt.

It should be mentioned that the conclusions on the nature of the RDS of the HOR, even for Pt, are still controversial. For example, Conway and Tilak[84] indicated that "there seems to be no dispute regarding the mechanism of the HOR on Pt (and

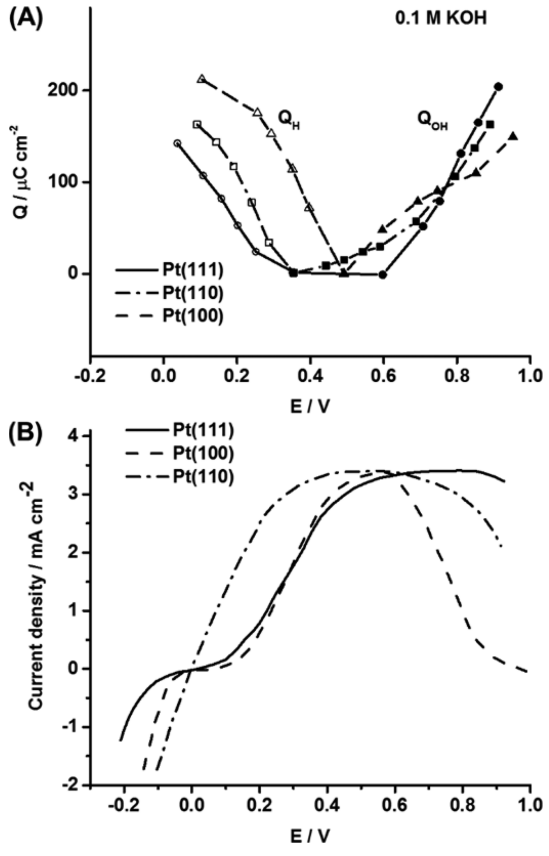


**Figure 9.** (A) Plots of the charge associated with the underpotential deposition of hydrogen and adsorption of hydroxyl species on Pt(*hkl*). (B) Polarization curves for the HOR on Pt(*hkl*) in 0.1 M KOH at 3600 rpm. Reprinted with permission from ref 46. Copyright 1996 Royal Society of Chemistry.



DOI: 10.1021/acscatal.8b00689
ACS Catal. 2018, 8, 6665−6690

Pt-alloys) being rate-determining dissociative adsorption of $H_2$", referring to other studies[50,51] to provide rationale for the statement. Vogel et al.[50] and Ross and Stonehart[51] have shown that the electrochemical reaction rate parameters are the same on smooth Pt, unsupported Pt black, and Pt crystallites supported on graphitized carbon. This correlates with the $H_2-D_2$ exchange in the gas phase both with and without chemisorbed carbon monoxide and is dependent only upon the surface area of the platinum catalyst. Therefore, the RDS for hydrogen molecule oxidation on Pt was assumed to be the dual-site dissociative chemisorption of the hydrogen molecule ($H_2 \rightarrow 2H^+$, i.e., the Tafel reaction). In recent work, Zheng et al.[39] and Bhowmik et al.[77] are inclined to directly relate the HBE value, which is considered to be linearly dependent on the $H_{UPD}$ desorption potential, to the HOR current density in basic media. This means that the Volmer reaction is considered to be the hydrogen oxidation reaction RDS. Since the surfaces of real catalysts comprise sites with different specific activities (or turnover frequencies), an approach was proposed to correlate the HOR activity and the number of active sites with similar HBE.[61]

$H_{UPD}$ desorption profiles for Ir/C catalysts were deconvoluted into three peaks (likely to be for the (110), (111), and (100) facets in the order of increase of the $H_{UPD}$ desorption peak).[103] The population of sites with the lowest HBE, namely, Ir(110) with an HBE value of −0.33 eV, was suggested to be responsible for the HOR. As shown by Sheng et al.,[83] the HOR activity for polycrystalline Pt obtained using the RDE method is found to decrease with the pH. At same time, the HBE obtained from cyclic voltammograms (CVs) linearly increases with the pH in buffer solutions (pH from 0 to 13) with the slopes of −10 meV vs RHE per pH unit for Pt(110) and −8 meV vs RHE per pH unit for Pt(100).

The universal correlation between $i_0$ and HBE, which was directly derived from the $H_{UPD}$ desorption potential value, observed on Pt/C, Ir/C, Pd/C, and Rh/C catalysts (Figure 10)[39] indicates that the HOR on those metals may share the same reaction mechanism. Zheng et al.[39] assume that the HOR proceeds via the ***T−V*** pathway, with the Volmer reaction being the RDS, and that the mechanism through which pH affects HBE is likely to be metal-independent. However, Santos et al.[104] showed that even though no $H_{UPD}$ signal is registered on Sn-rich Pt−Sn catalytic systems, they show higher exchange current density values compared with monometallic Pt.

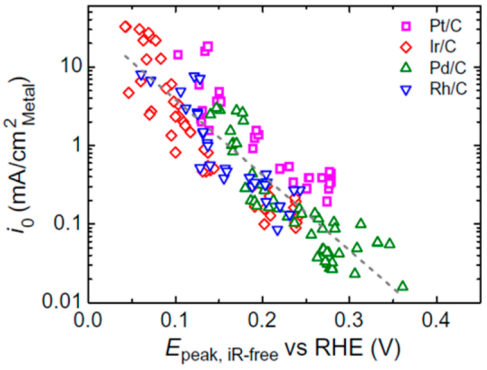


**Figure 10.** Correlation between the HOR/HER exchange current density on Pt/C, Ir/C, Pd/C, and Rh/C and the $H_{UPD}$ desorption peak potential. Reprinted from ref 39.

In summary, in this section the effect of $H_{OPD}$ on the kinetics in the potential range of hydrogen oxidation has been ruled out. The section has discussed the role of $H_{UPD}$, which is experimentally detected only for certain catalytic materials such as Pt, Rh, Pd, Ru, Ir, and Mo and, to the best of our knowledge, is not detected on Ni-based materials. Thorough literature analysis revealed two main contradicting hypotheses on the role of $H_{UPD}$ in the HOR, namely, $H_{UPD}$ as the intermediate involved in the Volmer mechanism versus $H_{UPD}$ as the blocking intermediate, with the second hypothesis being more likely.

## 4. HOR ELECTROCATALYSTS

**4.1. Overview of Different Material Classes.** This section summarizes the main types of the HOR electrocatalysts for alkaline media that have been investigated hitherto. Figure 11 shows the element-based classification used in the present review to discuss the characteristics and opportunities for these different state-of-the-art PGM and non-PGM HOR electrocatalysts.

*4.1.1. Platinum-Based Catalysts.* As evidenced by the activity values presented in Tables S2 and S3, platinum is the most active catalyst for the HOR in terms of exchange current density (Table S2) or mass activity at low overpotential ($\eta$ = 0.05 or 0.1 V) (Table S3). Different forms of Pt-based catalysts were investigated to catalyze the HOR in basic electrolytes, including Pt(*hkl*) single-crystal facets,[97] bulk/polycrystalline Pt,[49] carbon-supported Pt,[39,40,45] Pt−metal alloys,[6,105] Pt adlayers/islands,[40] and core−shell structures.[41,106]

Despite numerous studies on Pt-based materials, the details of the HOR mechanism and the nature of the rate-determining step are still debated. The controversy arises over the magnitude of the exchange current density $i_0$ (discussed in section 2), the predominant mechanism (***T−V***, ***H−V***, or dual-path ***T−V*** + ***H−V***), and the nature and coverage of the reactive intermediate $H_{ad}$ (see section 3.3). Conway and Tilak[84] summarized kinetic data for the HOR and concluded that the HOR rate on Pt is determined by the dissociative adsorption of $H_2$. Since they did not observe a pH effect on the HOR kinetics on Pt when measured at different pH > 4 (Figure 12), Bagotzky and Osetrova[62] came to the same conclusion.

The HOR rate on a smooth Pt surface was shown to be close to the rate of hydrogen dissociation (i.e., the rate of $H_2-D_2$ exchange) measured in the gas phase (Figure 13).[51] These results indicate that the electrolyte (in the pH range below 4) and/or the electrified interface does not affect the nature of the potential energy along the hydrogen−platinum reaction coordinate. This also leads to the conclusion that the HOR mechanism over smooth Pt is likely a slow dual-site dissociative adsorption of a hydrogen molecule followed by fast electrochemical oxidation of $H_{ad}$ to $H_3O^+$.

The HOR kinetics on Pt(pc) in 1 M KOH fits a direct discharge mechanism identical to the overall reaction $H_2 + 2OH^- \rightleftarrows 2H_2O + 2e^-$.[49] It seems that the step of extracting two electrons directly from $H_2$ is slow, with an exchange current density of 0.233 mA cm$^{-2}$. Since essentially identical values of the HOR specific exchange current density (0.69 ± 0.01 vs 0.57 ± 0.07 mA cm$^{-2}$; Table S2), activation energy (28.9 ± 4.3 vs 29.5 ± 4.0 kJ mol$^{-1}$), and charge transfer coefficient are observed on Pt(pc) and Pt/C, it was hypothesized that there is no significant effect of the Pt particle size on the HOR in 0.1 M KOH.[38] In contrast, Stonehart and Lundquist[75] reported a crystallite size effect for the oxidation of


DOI: 10.1021/acscatal.8b00689
ACS Catal. 2018, 8, 6665−6690

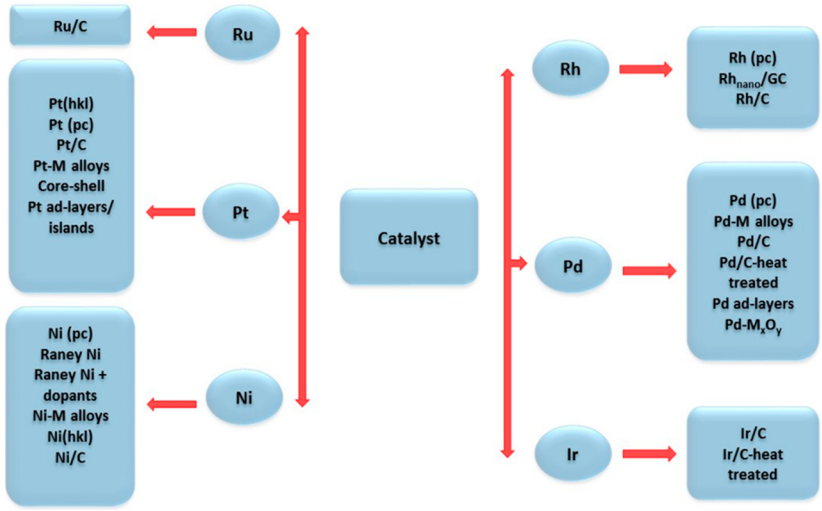


**Figure 11.** Description of the state-of-the-art PGM and non-PGM HOR electrocatalysts for use in basic media.

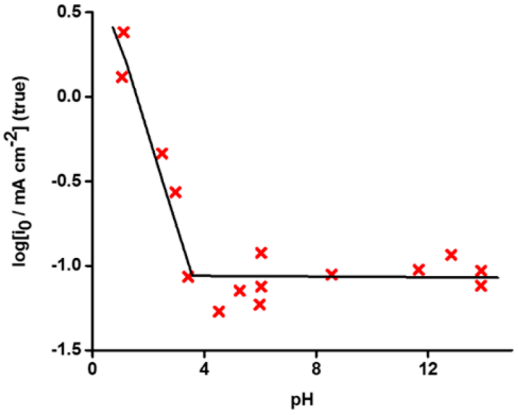


**Figure 12.** Dependence of the logarithm of the exchange current density for the HOR/HER (log $i_0$) on Pt(pc) as a function of the solution pH. Reprinted with permission from ref 62. Copyright 1973 Elsevier.

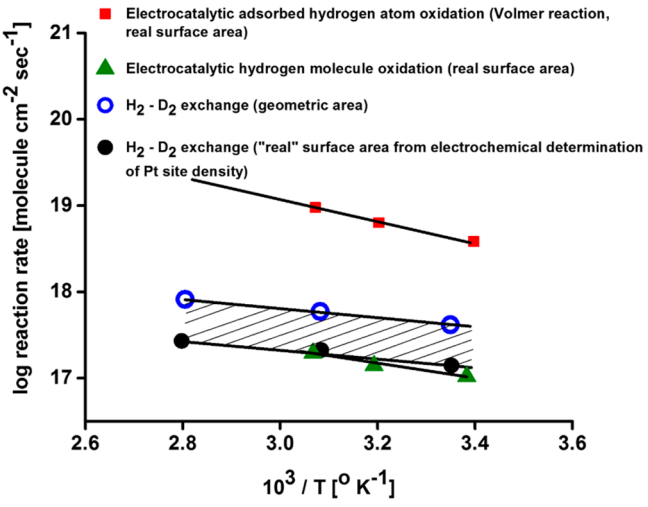


**Figure 13.** Comparison of absolute reaction rates for electrocatalytic hydrogen molecule oxidation and adsorbed hydrogen atom oxidation on platinum with the rate of gas-phase $H_2$–$D_2$ exchange. Reprinted with permission from ref 51. Copyright 1975 Research Institute for Catalysis.

preadsorbed hydrogen atoms on Pt. If this reaction were rate-determining (and most likely it is not), a crystallite size effect would be expected for hydrogen molecule oxidation. Poltorak and Boronin[107] showed that there is no crystallite size effect for the gas-phase rate of hydrogen dissociation, and therefore, one may not expect a crystallite size effect for the overall HOR. The exchange current density for hydrogen molecule oxidation calculated from the electrochemical rate constant equals that calculated from the gas-phase hydrogen dissociation rate constant.[107] Since hydrogen dissociation is the RDS in hydrogen molecule oxidation according to the study by Poltorak and Boronin[107] and since hydrogen dissociation takes place only on Pt, hydrogen spillover from Pt to the carbon substrate does not influence the rate of the hydrogen oxidation. It was also discussed that the specific reaction rates for unmodified Pt and Pt supported on carbon agree with the RDS being the dissociation reaction.[50] Thus, on the basis of literature analysis, we conclude that the dominant mechanism of the HOR on Pt is most likely the dissociative chemisorption of hydrogen (Tafel mechanism).

The HOR kinetics in alkaline solution is sensitive to the surface structure, as experimentally proven for the first time on Pt(111), Pt(100), and Pt(110) single-crystal surfaces (Figure 9).[46] The authors proposed that the kinetic differences arose mainly from the structure sensitivity of $H_{UPD}$ and $OH_{ad}$ with respect to the crystalline orientation of the surface and in turn from the roles of $H_{UPD}$ and $OH_{ad}$ in the HOR mechanism.[46] On Pt(110), the HOR occurs even on a surface fully covered by $H_{UPD}$.

Irrespective of the pH of solution, the HOR was shown to be structure-sensitive on various Pt(*hkl*) surfaces. At a temperature of 2 °C, Pt(110) ($i_0$ = 0.125 mA cm$^{-2}$) is 2.5 times more active than Pt(100) ($i_0$ = 0.05 mA cm$^{-2}$) and 12 times more active than Pt(111) ($i_0$ = 0.01 mA cm$^{-2}$).[97] At higher temperatures, the values of $i_0$ for Pt(110) and Pt(111) differ by less than a factor of 2. The authors[97] also assumed that the dependence of the activity on the crystal face can be attributed to the structure-sensitive adsorption of $H_{UPD}$ and $OH_{ad}$ and the effect these species have on the formation of the electroactive intermediate, $H_{OPD}$. The significant difference of the HOR kinetics for Pt(110) in alkaline electrolytes ($i_0$ = 0.125 mA cm$^{-2}$ at 2 °C)[97] versus acid electrolytes ($i_0$ = 0.65 mA cm$^{-2}$ at 1 °C)[108] seems to arise mainly from the presence of $OH_{ad}$ even close to 0 V vs


DOI: 10.1021/acscatal.8b00689
ACS Catal. 2018, 8, 6665−6690

RHE in alkaline electrolytes. In contrast to acidic solutions ($i_0$ increases from 0.65 to 1.35 mA cm$^{-2}$ as the temperature is increased from 1 to 60 °C for Pt(110), with a corresponding $E_a$ of 9.5 kJ mol$^{-1}$),[108] the activity in alkaline solutions is more strongly dependent on the temperature. In alkaline media, $i_0$ on Pt increases from 0.125 to 0.675 mA cm$^{-2}$ as the temperature is increased from 1 to 60 °C, with a corresponding $E_a$ of 23 kJ mol$^{-1}$. The monotonic correlation between the HBE and solution pH (the value of $\Delta H_{H_{ad}} = -FE H_{UPD}$ decreases linearly with a slope of −10 meV vs RHE per pH unit for the Pt(110) peak of the Pt/C catalyst) as well as that between the HOR rate and solution pH in multiple buffers over a wide range of pH suggested that the HBE governs the HOR activity (Figure 14).[83]

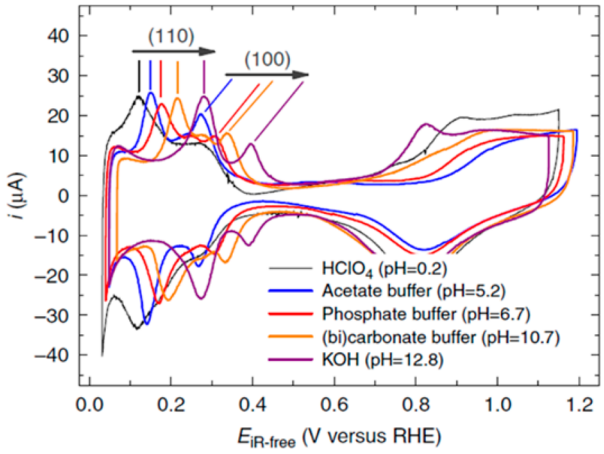


**Figure 14.** Steady-state CVs of Pt at several solution pH values collected in selected Ar-saturated electrolytes at a sweep rate of 50 mV s$^{-1}$. Reprinted with permission from ref 83. Copyright 2015 Springer Nature.

Moving further in the group of Pt-based HOR catalysts, Ru@Pt core−shell nanocatalysts with one or two Pt monolayers were also investigated.[106] The two- and one-ML-thick Pt shells on Ru exhibited enhanced (up to ca. 3-fold) surface-specific activity ($i_0$ = 1.49 and 1.10 mA cm$^{-2}_{Pt}$, respectively) compared with the Pt nanocatalyst (0.47 mA cm$^{-2}_{Pt}$) in basic solution.

These results differ considerably from observations in acidic media, with enhancement factors of 1.0 (180 mA cm$^{-2}_{Pt}$) and 0.4 (74.8 mA cm$^{-2}_{Pt}$), respectively, for Ru@Pt (1 ML) and Ru@Pt (2 ML) compared with 46% Pt/C (180 mA cm$^{-2}_{Pt}$). The authors[106] showed that in going from acid to base, the activation energy ($E_a$) increases most for the Volmer reaction and assumed that this results in the switch of the RDS from the Tafel reaction to the Volmer reaction. The increments in the activation energy ($\Delta E_a$) are 355 meV (or 34.3 kJ mol$^{-1}$) for the Pt catalyst and 315 meV (or 30.4 kJ mol$^{-1}$) for the Ru@Pt (2 ML) catalyst, i.e., close to the activation free energies for the Volmer reaction, which is the RDS in the dominant pathway.

Also considered in the group of Pt-based HOR catalysts, Au@Pt core−shell catalysts were also studied for the HOR in basic media. Au@Pt was synthesized by galvanic displacement.[40] In 0.1 M KOH, the Au@Pt surface exhibited the HOR specific activity similar to that of bulk Pt (0.66 mA cm$^{-2}_{Pt}$) and far superior to that of a pure Au disk (5.8 × 10$^{-3}$ mA cm$^{-2}_{Au}$). Au@Pt exhibits an activity similar to that of Pt supported on carbon (0.47 mA cm$^{-2}_{Pt}$). A true Pt monolayer on an Au support would increase the HBE as a result of the expansive strain on the Pt overlayer.[109] This in turn would decrease the activity of the catalyst. However, the results showed no decreased activity for Au@Pt catalysts.[109] The alkaline CO stripping data, which illustrate that the Au@Pt surface closely resembles bulk Pt, also support the idea that Pt does not form a true monolayer on the Au surface. These results are scarce attempts to fundamentally understand the catalyst design. They shed some light on the surface strain effect on the catalytic activity of monolayers and tried to correlate the experimental data with the theoretical predictions of HBE values (Table S1).

Platinum-coated copper nanowires (Pt/CuNWs) synthesized by the partial galvanic displacement of CuNWs, Cu-templated Pt nanotubes (PtNT(Cu)), a 5% Cu monolayer on a bulk polycrystalline Pt electrode (5% ML Cu/Pt(pc)), Pt(pc), and carbon-supported Pt were studied as HOR catalysts in 0.1 M KOH.[41] Comparison of these catalysts demonstrates that the inclusion of Cu benefited the HOR specific activity of Pt/CuNWs ($i_0$ = 2.03 mA cm$^{-2}_{Pt}$), likely by providing compressive strain on Pt; surface Cu further aids in hydroxyl adsorption, thereby improving the HOR activity of the catalyst. Pt/CuNWs exceed by 3.5 times the surface-specific exchange current density of carbon-supported Pt ($i_0$ = 0.59 mA cm$^{-2}_{Pt}$). The use of the 5% ML Cu/Pt(pc) catalyst ($i_0$ = 1.64 mA cm$^{-2}_{Pt}$) improved the HOR activity of Pt(pc) ($i_0$ = 0.71 mA cm$^{-2}_{Pt}$). The observed improved performance seems to be largely driven by the electronic tuning provided by the Cu substrate and Cu impurities within the Pt shell.[41]

The activity of platinum-based catalysts in the HOR spans the range of 1.4−1.7 mA cm$^{-2}_{real}$ ($\eta$ = 0.05 V) for Pt/C, Pt(pc), and Pt−dopant and varies from 80−150 A $g_{Pt}^{-1}$ for Pt−dopant up to 900−1000 A $g_{Pt}^{-1}$ ($\eta$ = 0.05 V) for Pt/C.

The stability of Pt electrocatalysts in alkaline media has, surprisingly, been little investigated hitherto. Accelerated stress tests combining electrochemical measurements and identical-location transmission electron microscopy (ILTEM) studies on Pt/C nanoparticles were conducted in a liquid alkaline electrolyte (0.1 M KOH at 25 °C)[110,111] and in a solid anion-exchange polymer electrolyte using a "dry cell".[111] It was shown that Pt/C is more stable when operated at the AEM interface than in liquid alkaline electrolytes.[111] However, the accelerated stress tests and reported stability data[110,111] have hitherto mimicked cathode operation.

*4.1.2. Palladium-Based Catalysts.* RDE measurements on 10% Pd/Vulcan XC72 (Premetek) revealed (Figure 2) that the value of the exchange current density, determined from both Butler−Volmer fitting and the micropolarization region, is 90 times lower in 0.1 M NaOH (0.06 ± 0.02 mA cm$^{-2}_{Pd}$ at 40 °C) than in an acidic medium with pH = 0 (5.2 ± 1.2 mA cm$^{-2}_{Pd}$).[45] Because of the significant decrease in $i_0$ with increasing solution pH, the authors considered the Volmer step as the RDS on Pd/C. Zheng et al.[39] obtained similar $i_0$ values for 20% Pd/Vulcan XC 72 (Premetek) using the RDE method. At 20 °C K, the authors measured $i_0$ values of 0.04 and 0.77 mA cm$^{-2}_{Pd}$ in 0.1 M KOH (pH 12.8) and 0.1 M $HClO_4$ (pH 1.2), respectively.

As is the case for Pt, $i_0$ values measured by different groups for Pd catalysts are scattered (Table S2). The differences can arise not only from the different methods used to evaluate $i_0$ but also from the ones utilized to determine the surface area of the catalyst. For example, the surface area calculated from volume/area-averaged particle size from TEM for Pd/C was 148 m$^2$ g$^{-1}$, while the electrochemical surface area determined by cyclic voltammetry in 0.1 M KOH was 78 ± 8 m$^2$ g$^{-1}$ on the


DOI: 10.1021/acscatal.8b00689
ACS Catal. 2018, 8, 6665−6690

same catalyst and that determined by CO stripping in 0.1 M KOH was 96 $m^2$ $g^{-1}$.[39]

Since the absorption of hydrogen into the Pd bulk might complicate the quantification of the HOR activity on bulk polycrystalline Pd, the absorption of hydrogen can be circumvented by depositipn of thin overlayers onto non-absorbing substrates such as Pt, Rh, and Au.[112] Henning et al.[112] deposited adlayers of palladium on a polycrystalline Au substrate either by galvanic replacement of underpotentially deposited copper or by electrochemical plating from a $Pd^{2+}$ solution. The surfaces appear to consist of three-dimensional Pd structures of an unknown thickness that is believed to scale with the palladium coverage, $\theta_{Pd/Au}$. The $\theta_{Pd/Au}$ parameter was shown to be inversely proportional to the HOR activity of the Pd-on-Au surface in 0.1 M NaOH at 20 °C, in agreement with numerous theoretical and experimental studies in acidic media that correlate the effect of the tensile strain induced by the Au substrate on the Pd lattice (Table S2).

As fundamental studies of the HOR on bulk Pd crystals are complicated by the fact that the $H_{UPD}$ process is difficult to separate from $H_2$ absorption in the bulk of Pd, studies of Pd monolayers deposited on different substrates were used to determine the $H_{UPD}$ charge transfer resistance.[113] Using the $H_{UPD}$ CTR value of ca. 8000 Ω $cm^2$ in 0.1 M NaOH and eq 19, the $i_0$ value was estimated to be ca. 0.003 mA $cm^{-2}_{Pd}$. Thus, there is no quantitative agreement with the $i_0$ values (Table S2), which might serve as an indirect proof that $H_{UPD}$ is not an HOR intermediate.

The effect of the particle size of the Pd/C catalyst was studied in 0.1 M KOH.[114] The specific exchange current density for the HOR increases as the Pd particle size increases from 3 to 19 nm (Table S2) and then reaches a plateau with activity similar to that of bulk Pd.[114] The authors hypothesized that the enhanced surface-specific activity with increasing particle size could be attributed to the increased ratio of the sites with weaker HBE, as revealed in cyclic voltammograms.

Another group of Pd-based catalysts, 4−9% Pd-containing "3020 anode" catalysts (Acta S.p.a., Italy), were compared to commercially available 5% Pd/C and 40% Pt/C catalysts (RDE, 0.34 $mg_{cat}$ $cm^{-2}$, 1 M KOH, 1600 rpm, Tokuyama Ionomer A3 as a binder). The company did not disclose the exact composition of their 3020 Pd-based catalyst. The results revealed that the catalytic activity of 3020 catalysts is in the range of 40−58 mA $mg_{Pd}^{-1}$ at 0.025 V vs RHE versus ca. 30 and ca. 25 mA $mg_{metal}^{-1}$ for the 40% Pt/C and 5% Pd/C catalysts, respectively, which shows the competitiveness of Pd to Pt. However, comparison of the reported data with those in Table S3 shows that Pd-based electrocatalysts still leave much to be desired.

In summary, analysis of the kinetic data on the HOR in basic media (Tables S2 and S3) shows that the average value of the exchange current density for Pd-based catalysts is ca. 0.05−0.1 mA $cm^{-2}_{Pd}$. The lowest values (<0.001 mA $cm^{-2}_{Pd}$) were obtained for strained layers of Pd on Au. The highest values (ca. 1.0 mA $cm^{-2}_{Pd}$) were reached for PdIr/C and 1.5% Pd/Ni. The surface-specific activity of Pd-based catalysts spans the range from 0.04 to 0.30 mA $cm^{-2}_{Pd}$ ($\eta$ = 0.05 V) for Pd/C and Pd(pc) up to 1.7−4.0 mA $cm^{-2}_{real}$ ($\eta$ = 0.05 V) for PdIr and $Pd_{ad}$/Au. Evidently, on the basis of the available literature data, similarly to Pt, the HOR kinetics on Pd is pH-dependent, which either can be the result of the hypothesized Volmer mechanism or, more likely, is related to the $OH_{ad}$ surface coverage effect. The latter was studied on Pt facets but has not been shown experimentally on Pd facets, bulk Pd and Pt, or supported/unsupported nanoparticles of Pd and Pt.

Whereas Pd/C nanoparticles suffer dramatic degradation in an acidic medium (0.1 M $H_2SO_4$), accelerated stress tests combining electrochemical measurements with ILTEM studies have demonstrated their higher stability in 0.1 M KOH (25 °C)[115] as opposed to Pt/C.[110,111] However, alkaline electrolytes containing reducing species (hydrogen, hydrazine borane) were found to result in a slightly higher instability of Pd/C nanoparticles.[115] Kabir et al.[116] have shown that using a graphitized carbon support instead of an amorphous one did not significantly improve the stability of Pd/C in alkaline media.

*4.1.3. Ru-Based Catalysts.* Scarce studies on Ru catalysts can be found in the literature on the HOR in alkaline media. The surface-specific activity of Ru/C shows a volcano-shaped dependence on the particle size with a maximum activity at approximately 3 nm,[117] unlike Pd[114] and Ir-based catalysts,[61] where the increase in exchange current density is aligned with a particle size decrease. The authors showed that the HOR activity of approximately 3 nm Ru/C (0.64 mA $cm^{-2}_{Ru}$) is higher than that of commercially available Pt nanoparticles supported on carbon (0.34 mA $cm^{-2}_{Pt}$). The Ru nanoparticle structure was shown to change from an amorphous-like structure below 3 nm size to a metal nanocrystallite with a roughened surface at approximately 3 nm and then to a crystallite with well-defined facets above 3 nm size. It was proposed that the unique structure observed at this particular size, long-bridged coordinatively unsaturated Ru metal surface atoms on its nanocrystallite, is a key to achieve high HOR activity.[117] In spite of this specific study showing reasonable activity for Ru at this specific particle size, the general drawback of pure Ru catalysts is that oxygenated species on Ru inhibit $H_2$ adsorption, and consequently, the HOR current decreases above 0.2 V (Figure 15). To date, no rational approach has been proposed to circumvent the electrochemical oxidation of the Ru surface.

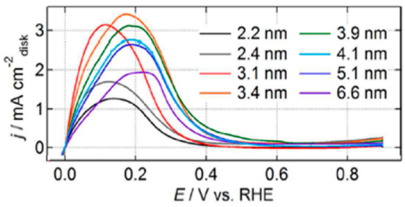


**Figure 15.** HOR polarization curves obtained on Ru/C catalysts in 0.1 M NaOH aqueous solution. Sweep rate, 10 mV $s^{-1}$; rotation rate, 2500 rpm; temperature, 25 °C. Reprinted from ref 117. Copyright 2013 American Chemical Society.

*4.1.4. Ir-Based Catalysts.* Unlike Pt and Pd, much less attention has been paid to studies of iridium catalytic activity in the HOR in alkaline media. Zheng and collaborators showed with Ir/C that the fraction of Ir sites having a low HBE increased with increasing particle size (in the range of 3−12 nm) (Table S1).[61] This resulted in a negative correlation between the fraction of low-HBE sites and the electrochemical specific surface area (Figure 16). The HOR activities normalized to the surface area of the lowest-HBE site are independent of the total electrochemical surface area, indicating that those sites with low HBE (most likely low-index facets) are the most active sites for the HOR. Therefore, it was suggested[61]



DOI: 10.1021/acscatal.8b00689
ACS Catal. 2018, 8, 6665−6690

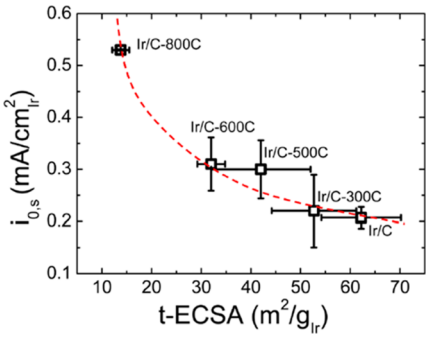


**Figure 16.** Exchange current densities for the HOR on Ir/C samples normalized to the electrochemical surface area (t-ECSA) as a function of t-ECSA. Reprinted from ref 61. Copyright 2015 American Chemical Society.

that extended Ir nanostructure with a high fraction of low-index facets, such as Ir nanotubes or nanowires, may have higher HOR surface-specific activities than small Ir nanoparticles. A similar effect was observed by the same research group for Pd nanoparticles (as discussed in section 4.1.3).[114] Ru particles showed a volcano-type dependence of the HOR activity on the particle size,[117] and the activity is also related to the surface crystal structure. The size effect of Pt, which has been much more extensively studied and was discussed above, is not in agreement with the hypothesis about the predominant role of low-index facets in the HOR.

Calculations made by Montero et al.[95] showed that the HOR on Ir takes place mainly through the ***T*−*V*** route, with a small contribution of the ***H*−*V*** route for nanostructured iridium prepared by sputtering on a glassy carbon substrate. In the potential range between $-0.015 \leq \eta/V \leq 0.30$, the reaction rates of the Tafel step ($V_T$) in alkaline and acidic solutions were suggested to be close. This statement was confirmed from the values obtained for Ir electrodes in alkaline solution ($2.02 \times 10^{-9}$ mol s$^{-1}$ cm$^{-2}$) and acidic solution ($6.92 \times 10^{-9}$ mol s$^{-1}$ cm$^{-2}$).[118] With respect to the values of the reaction rates of the Heyrovsky and Volmer steps, it is straightforward that they should be different for alkaline and acidic solutions. In order to explain this difference, Montero et al.[95] proposed the following speculative model. In acidic solutions, in both steps a proton is incorporated into the water network as an electron is transferred to the metallic substrate. In contrast, in alkaline solutions the electron transfer goes along with the disappearance of a hydroxyl ion. The authors[95] assumed that both species enter or leave the reaction plane by a Grotthuss-type mechanism, which implies the transfer of hydrogen bonds through a highly ordered water network. In this case, it is more difficult for $OH^-$ than for $H^+$ to achieve the appropriate spatial configuration to enable the electron transfer. This fact implies an increase in the activation energy of the ***V*** step in alkaline solution and therefore a decrease in the corresponding equilibrium reaction rate ($V_V = 1.19 \times 10^{-8}$ mol s$^{-1}$ cm$^{-2}$ in base vs $9.89 \times 10^{-5}$ mol s$^{-1}$ cm$^{-2}$ in acid).[118]

The exchange current density values of polycrystalline iridium-based catalysts in the HOR span the range of 0.2−0.5 mA cm$^{-2}_{Ir}$, which places Ir on the same level as polycrystalline Pt. Although these results are of high fundamental importance, iridium catalysts are unaffordable economically because of the scarcity of the element (Ir is the rarest element among the PGMs).

*4.1.5. Rh-Based Catalysts.* There have been a few studies of the HOR on Rh, including both basic and acidic solutions (the data in acid are analyzed here only for the sake of comparison). In Montero's study of the HOR kinetics on Rh in basic solution (0.2 M NaOH, 25 °C),[119] it was shown that the reaction proceeds mainly through the ***T*−*V*** route given Frumkin-type adsorption of the reaction intermediate, $H_{ad}$, with the following kinetic parameters: Tafel reaction rate $V_T = 1.128 \times 10^{-9}$ mol s$^{-1}$ cm$^{-2}$, Heyrovsky reaction rate $V_H = 1.461 \times 10^{-16}$ mol s$^{-1}$ cm$^{-2}$, and Volmer reaction rate $V_V = 2.667 \times 10^{-9}$ mol s$^{-1}$ cm$^{-2}$ in the overpotential range $-0.015$ V $< \eta <$ 0.40 V. The exchange current density value was reported to be 0.118 mA cm$^{-2}$. For the sake of comparison, the HOR on the same catalyst in an acidic medium (0.5 M $H_2SO_4$ at 25 °C) proceeds simultaneously through the ***T*−*V*** and ***H*−*V*** routes.[119] The corresponding reaction rates are $V_T = 1.257 \times 10^{-9}$ mol s$^{-1}$ cm$^{-2}$, $V_H = 6.083 \times 10^{-9}$ mol s$^{-1}$ cm$^{-2}$, and $V_V = 5.546 \times 10^{-8}$ mol s$^{-1}$ cm$^{-2}$ in the overpotential range $-0.015$ V $< \eta <$ 0.25 V, and the exchange current density is 0.677 mA cm$^{-2}$. Thus, the HOR kinetics on Rh is significantly influenced by the pH: $V_H$ and $V_V$ in 0.5 M $H_2SO_4$ are ca. 6 and 1 order of magnitude higher than those in 0.2 M NaOH. The rate constant for non-electrochemical $H_2$ dissociative adsorption, $V_T$, is slightly affected by pH, similarly to Ir.[118] According to Montero's calculations,[119] the Tafel step is the RDS of the HOR in alkaline solution, as opposed to ref 39, where the authors claim the Volmer mechanism for the HOR on Rh.

The specific activities of rhodium-based catalysts in the HOR span the range of 0.5−0.9 mA cm$^{-2}_{real}$ ($\eta$ = 0.05 V). The exchange current density values of Rh-based catalysts in the HOR vary in the range of 0.1−0.35 mA cm$^{-2}_{Rh}$.

*4.1.6. Nickel-Based Catalysts.* Ni-based catalysts have been extensively studied for the HOR in basic media and at present remain the only non-PGM HOR electrocatalysts with significant activity. One can distinguish several groups of catalytic materials having metallic nickel as the main component. Among them, there are metal-doped-sponge Raney nickel catalysts,[120−133] electrochemically deposited bulk double- and ternary-metal catalysts,[134] highly dispersed supported Ni-based catalysts,[20] and single-crystal Ni facets.[81] The first group, Raney nickel catalysts, is the most popular, with the highest number of studies, because of its popularity in liquid electrolyte (KOH)-based alkaline fuel cells.

Raney Ni was shown to be a comparatively active non-noble material for the HOR in gas diffusion electrodes (GDEs). However, the catalytic activity and stability of Raney Ni alone as a base metal for this reaction is limited.[131] These problems have been partially overcome by doping of transition metals, such as Ti,[121,123,135] La,[136] Cr,[135] Fe,[122] Co,[122,124,126] Cu (mostly as a conducting additive),[137] and Mo,[121,138] into the Ni−Al alloy at loadings of a few percent prior to extraction by KOH. The resultant Raney nickel catalysts are pyrophoric because of the $H_2$ evolution during Al leaching and therefore must be handled accordingly,[130] as the nickel is loaded with 0.5−1.2 hydrogen atoms per nickel atom. Even if the surface area can exceed 60 m$^2$ g$^{-1}$ depending on the Ni preactivation procedure,[130,132,133,139] the Ni particle size is within the micrometer range—from several micrometers to several tens of micrometers[123]—which makes Raney nickel inapplicable for nanoscale purposes. The Raney nickel catalyst loadings for the conventional double-layered GDEs are 20−100 mg cm$^{-2}$ with layer thicknesses of up to 300 $\mu$m.[135]


DOI: 10.1021/acscatal.8b00689
ACS Catal. 2018, 8, 6665−6690

Moreover, Raney Ni is functional under very high alkalinity (6 M KOH) as the catalyst of thick double-layered GDEs, and it is not catalytically active for an AEMFC, which can be mimicked as 0.1−1 M KOH.[20] It was found that in an AEMFC, the hydrogen anode made from such Ni catalysts showed an electrode potential characteristic of nickel oxides instead of the potential of a hydrogen electrode, and this fact was also confirmed by other recent studies.[140−142] The electrolysis method used in alkaline fuel cells (with liquid electrolyte) to activate the Ni anode in a separate electrolyzer (electrolysis as a hydrogen evolution electrode)[139] is inapplicable for AEMFCs using a membrane-electrode-assembly (MEA) structure unless a proper bifunctional ORR/OER catalyst is used on the cathode, implying the use of a carbonless support.

Disregarding the difficulties of directly applying Raney nickel catalysts to AEM-based electrodes, attention should be paid to certain experimental results for the further development of a new generation of Ni-containing catalysts for the HOR. The polarization resistance, $\omega$, which is the slope of the HOR polarization curve measured on a thick double-layer GDE and is used as one of the criteria of the catalytic activity, was shown to be in the range of 0.1−0.3 Ω cm$^2$.[135] The linear dependence of $\omega$ on $1/T$ allowed an estimate of the apparent value of the HOR activation energy, which was shown to be 34.5 and 31.6 kJ mol$^{-1}$ for 0.8% Cr@Ni and 0.8% Ti@Ni, respectively.[135] Close values of 28−32 kJ mol$^{-1}$ were also obtained for copper oxide-doped Raney nickel GDEs by Alsaleh,[137] who analyzed the dependence of the exchange current density $i_0$ on the temperature. The $i_0$ value, estimated according to the mathematical model developed by Celiker et al.,[143] was shown to be 111.5 mA cm$^{-2}$ at 65 °C. Other values within the temperature range of 25−75 °C are presented in Table S2. Ewe et al.[144] found that the catalytic properties of Ti doped with Raney Ni (for hydrogen anodes of alkaline fuel cells) could be improved by an $\alpha$-Ni(OH)$_2$ surface coating, which is obtained by carefully optimized oxidation. It was observed that an $\alpha$-Ni(OH)$_2$ content of 5−6% increased the attainable current density by a factor of 3 to 4.

The quantitative analysis of the overpotential−current density dependence for the HOR on the Raney Ni GDE is partially presented in Table S3. Benchmarks of the HOR mass activities at 0.05 V vs RHE on the PGM-free catalysts were also presented by Zhuang et al.[42]

Tertiary Ni alloys were also studied for the HOR in alkaline media. A metallic CoNiMo catalyst electrochemically deposited on a Au(pc) disc was shown to exhibit high HOR activity (20-fold higher than that of Ni).[134] Density functional theory (DFT) calculations and parallel $H_2$ temperature-programmed desorption (TPD) experiments on structurally much simpler model alloy systems showed a trend that CoNiMo has an HBE similar to that of Pt (CoNi/Mo(110), −0.43 eV; Pt(111), −0.46 eV) and much lower than that of Ni (Ni(111), −0.51 eV). This suggests that the formation of multimetallic bonds modifies the HBE of Ni and is likely a significant contributing factor for the enhanced HOR activity.[134] The apparent value of the activation energy for the ternary CoNiMo catalyst was determined to be 35 ± 1 kJ mol$^{-1}$, compared with 29 ± 1 kJ mol$^{-1}$ for a Pt disc, which is in good agreement with measurements done on Raney nickel electrodes.[92] The values of $i_0$ are also presented in Table S2.

A composite catalyst developed by Zhuang et al.[42]—Ni nanoparticles supported on nitrogen-doped carbon nanotubes (Ni/N-CNT)—can achieve hydrogen oxidation activity of 9.3 A g$^{-1}$ at 0.05 V at room temperature in 0.1 M KOH. This is probably the highest value known to date for Ni-based catalysts. Although nitrogen-doped carbon nanotubes are a very poor hydrogen oxidation catalyst, as a support they increase the catalytic performance of nickel nanoparticles by a factor of 33 (mass activity) or 21 (exchange current density) relative to unsupported nickel nanoparticles,[42] as shown in Table S2. In their DFT calculations, Zhuang et al.[42] showed that the nitrogen-doped support stabilizes the nanoparticle against reconstruction, while nitrogen located at the edge of the nanoparticle tunes local adsorption sites by affecting the d orbitals of Ni.

The electrocatalytic behavior of low-index nickel single-crystal electrodes for hydrogen oxidation was discussed in relation to the crystallographic structure of the electrode surface and the pH of the electrolyte solution by Floner et al.[81] These authors showed that whereas small structural effects are displayed during surface oxidation and formation of $\alpha$-Ni(OH)$_2$, a strong dependence of the hydrogen oxidation rate on the crystal structure is observed in alkaline media. Ni(100) and mainly Ni(110) are the most active structures (5 to 6 times more active than polycrystalline nickel). The reactivity of hydrogen on polycrystalline nickel is low, i.e. it is a slow process, visible only under quasi-stationary conditions. For the Ni(100) and Ni(110) planes, the current densities exhibit a maximum value at pH 13. A decrease in pH leads to a diminution in the HOR current, in contrast to the polycrystalline nickel. The activation energy at pH 9 is potential-independent and equal to 50 kJ mol$^{-1}$, while it is 40.2 kJ mol$^{-1}$ at pH 4.8. The intensities of the occupied orbitals at the Fermi level for the Ni(111), Ni(100), and Ni(110) surfaces are 2.0, 2.2, and 2.7 states eV$^{-1}$, respectively,[145] and therefore, the Ni(110) surface can donate a higher electron density to the adsorbate. The surface metal atom coordination numbers for the Ni(111), Ni(100), and Ni(110) surfaces are 9, 8, and 7, respectively, and one would therefore expect the strongest adsorption to occur on the Ni(110) surface.[146] Hence, on the basis of the differences in both electron density and coordination number, one would expect that the strength of the adsorption energies would decrease in the order Ni(110) > Ni(100) > Ni(111).

In view of the linear relation between the limiting diffusion current ($i_{lim}$) and the number of active sites, Angely et al.[147] suggested that the most probable HOR mechanism for Ni in alkaline media is $H_2 \rightleftarrows H_{2,ad}$ instead of dissociative adsorption ($H_2 \rightleftarrows 2H_{ad}$) as observed on Pt.

The highest mass-specific activities of nickel-based catalysts in the HOR are 13.6 A $g_{cat}^{-1}$ ($\eta$ = 0.05 V) for Raney Ni + $Ti_{0.8}$ and 9.33 A $g_{Ni}^{-1}$ ($\eta$ = 0.05 V) for Ni/N-CNT. The exchange current density values of Ni-based catalysts in the HOR vary in the range of $(1-28) \times 10^{-3}$ mA cm$^{-2}_{Ni}$.

In some scarce works devoted to the stability tests on PGM nanoparticles,[110,111,115] alkaline media were shown to be more aggressive than acidic ones. One might expect more drastic effects on non-noble electrocatalysts like Ni-based materials. However, Zadick et al.[148] demonstrated promising durability of a $Ni_3Co/C$ electrocatalyst for a 6 h long ammonia borane electrooxidation and in accelerated stress tests in 0.1 M NaOH. ILTEM experiments in particular demonstrated the absence of any consequent degradation of $Ni_3Co/C$. Moreover, the latter confirmed a much larger material (structural) stability than reported in the literature for carbon-supported Pd[115,116] and Pt[110,111] nanoparticles.



DOI: 10.1021/acscatal.8b00689
ACS Catal. 2018, 8, 6665−6690

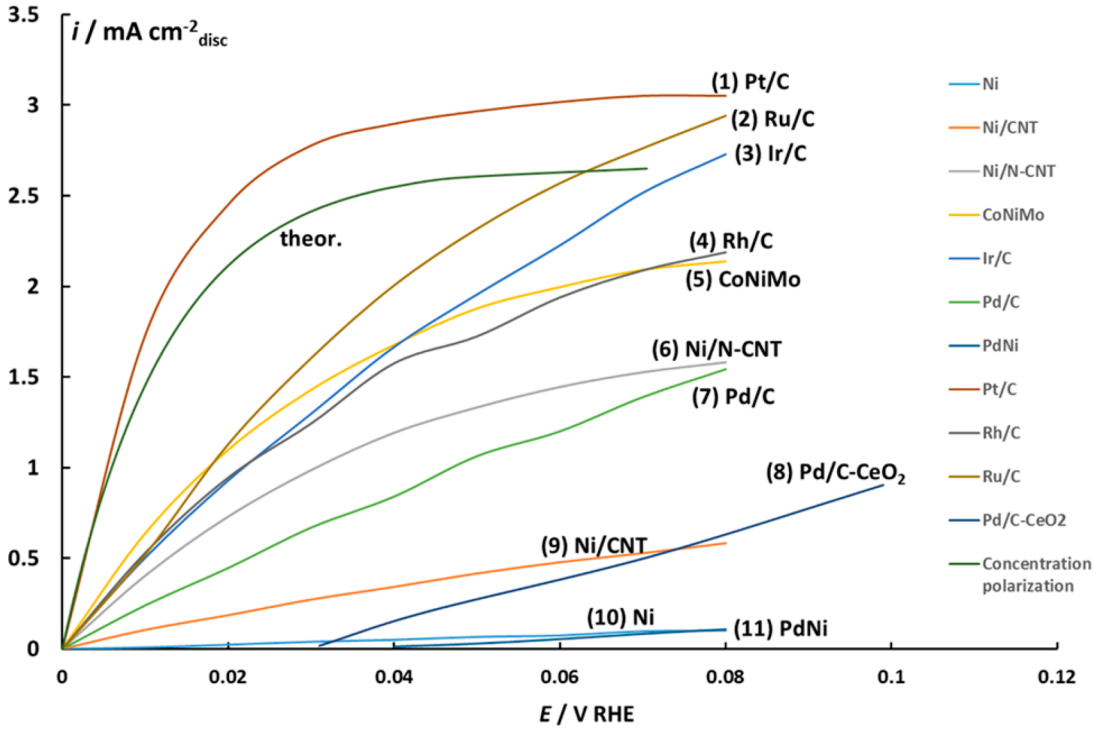


**Figure 17.** Comparison of the HOR polarization curves for different catalytic materials: (1) 5% Pt/C, 0.1 M NaOH, 40 °C, 1600 rpm, catalyst loading 2.5 $\mu g_{Pt}$ $cm^{-2}_{geom}$;[45] (2) 50% Ru/Vulcan XC-72R, 0.1 M NaOH, 25 °C, 2500 rpm, catalyst loading 10 $\mu g_{Ru}$ $cm^{-2}_{geom}$;[117] (3) 20% Ir/C, 0.1 M KOH, 20 °C, 1600 rpm, catalyst loading 5 $\mu g_{Ir}$ $cm^{-2}_{geom}$;[61] (4) 20% Rh/C, 0.1 M KOH, 20 °C, 1600 rpm, catalyst loading 2−20 $mg_{Rh}$ $cm^{-2}_{geom}$;[39] (5) CoNiMo, 0.1 M KOH, 20 °C, 1600 rpm, ca. 600 mg $cm^{-2}$;[134] (6) Ni/N-CNT, 0.1 M KOH, r.t., 2500 rpm, catalyst loading 0.25 $mg_{Ni}$ $cm^{-2}_{geom}$;[42] (7) 20% Pd/C, 0.1 M KOH, 20 °C, 1600 rpm, catalyst loading 5 $\mu g_{Pd}$ $cm^{-2}_{geom}$;[61] (8) Pd/C−$CeO_2$, 0.1 M KOH, 1600 rpm, 6.5 $\mu g_{Pd}$ $cm^{-2}_{geom}$;[22] (9) Ni/CNT, 0.1 M KOH, r.t., 2500 rpm, catalyst loading 0.25 $mg_{Ni}$ $cm^{-2}_{geom}$;[42] (10) Ni, 0.1 M KOH, r.t., 2500 rpm, catalyst loading 0.25 $mg_{Ni}$ $cm^{-2}_{geom}$;[42] (11) PdNi (17% Pd coverage), 0.1 M KOH, 1225 rpm, 0.9 $\mu g$ $cm^{-2}_{disk}$.[71]

One of the other ways for straightforward and convenient comparison of the catalytic activities of different groups of the HOR electrocatalysts is the direct overlap of the HOR polarization curves measured under the same or close experimental conditions. In Figure 17 we present a comparison of some selected polarization curves recorded by the RDE method. Even though the experimental conditions such as catalyst loading, electrode rotation rate, and temperature are scattered, one can easily range the activity of the existing catalysts: Pt is the most active and the most expensive, along with Rh and Ir. However, Ru demonstrates competitive current densities, and at certain modifications (Ni/N-CNT) and high metal loadings (NiCoMo) non-PGM catalysts can be considered, in all certainty, as a future alternative for PGM-based electrocatalysts.

Analysis of the values of the surface-specific exchange current density (Table S2 and Figure 18) reveals that the most common ways to enhance the catalytic activity of monometallic systems are (1) catalyst modification by the introduction of a doping element into (1.1) bulk or (1.2) the surface (from islands up to several monolayers) via ligand or bifunctional mechanisms, (2) use of a substrate material that changes the strain of the particles, and (3) thermal treatment in order to modify the crystal structure. At room temperature, monometallic Pt nanoparticles have shown the highest $i_0$ (ca. 0.6 mA $cm^{-2}$) compared with other monometallic PGM systems (0.04−0.05 mA $cm^{-2}$ for Pd nanoparticles and 0.2−0.4 mA $cm^{-2}$ for Ir/C). Among the facets of Pt, the exchange current density decreases in the order Pt(110) > Pt(100) > Pt(111). Introduction of Ru, Fe, and Co results in PtM bimetallic

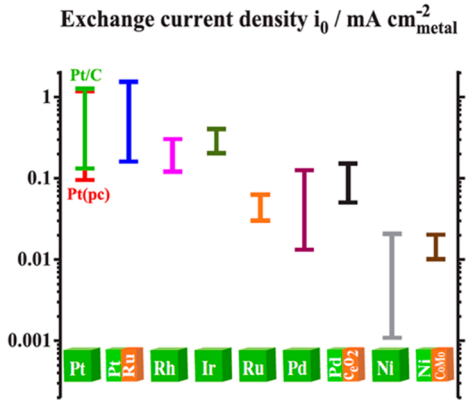


**Figure 18.** Ranges of experimental values of the exchange current density in the HOR for monometallic surfaces (green cubes) and for bifunctional catalysts (green-orange cubes).

systems with enhanced activity. Doping with Cu and Au leads to a decrease in $i_0$ compared with mono-Pt. A drastic increase in the Pt activity was gained from the fine modification of Cu nanowires by Pt layers (2.03 mA $cm^{-2}$) or adsorption of Ru monolayers on the surface of Pt nanoparticles (Ru@Pt 1 ML with $i_0$ = 1.49 mA $cm^{-2}$). Significant improvement of palladium was reached by galvanic replacement of nickel in nanoparticles by Pd (1.5% Pd/Ni with $i_0 \approx 1$ mA $cm^{-2}$) or introduction of Ir (PdIr with $i_0$ = 0.98 mA $cm^{-2}$). Ruthenium nanoparticles were reported to have low activity (0.03−0.06 mA $cm^{-2}$), and the Ru surface, as well as Ni, suffers from electrooxidation at overpotentials higher than 0.1 V. Raney Ni has extremely low



DOI: 10.1021/acscatal.8b00689
ACS Catal. 2018, 8, 6665−6690

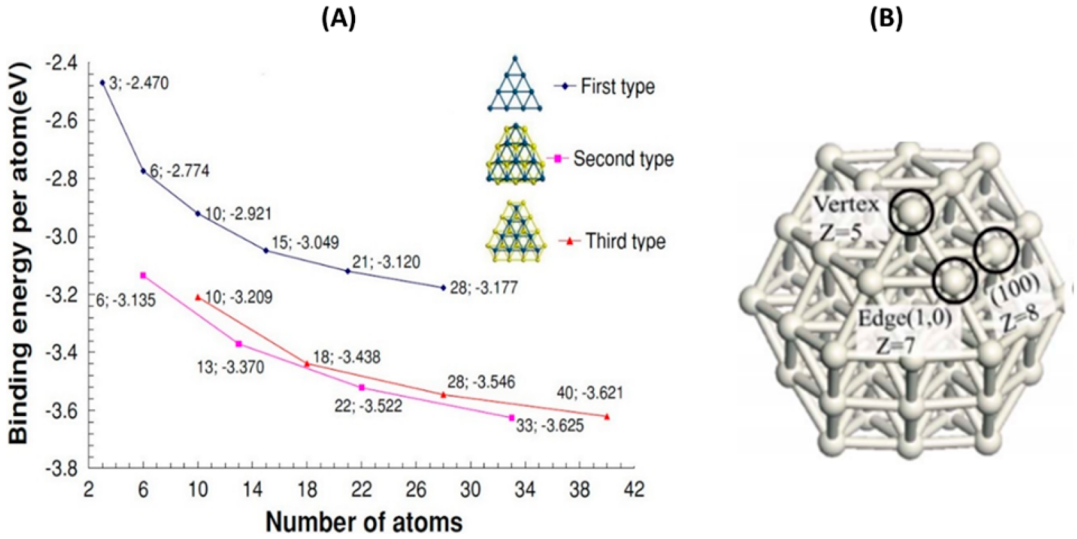


**Figure 19.** (A) OH binding energies (OHBEs) per atom for three selected types of Pt nanoclusters. (B) 1 nm Pt cluster. The coordination number $Z$ is the average nearest-neighbor coordination number of the Pt atoms. Reprinted with permission from ref 152. Copyright 2009 Springer Science +Business Media.

values of the exchange current density (ca. $5 \times 10^{-4}$). Doping of Raney nickel with Ti and Mo leads to a drastic change in the activity (ca. $2 \times 10^{-3}$ and ca. $9 \times 10^{-3}$ mA cm$^{-2}$, respectively). Recently, progress was made in the development of Ni-based catalysts that resulted in exchange current density values of $15 \times 10^{-3}$ mA cm$^{-2}$ (for NiCoMo) and even $28 \times 10^{-3}$ mA cm$^{-2}$ (for Ni/N-CNT).

**4.2. Bifunctional HOR Catalysis in Alkaline Media.** This section is devoted to bifunctional HOR catalysis, which we herein define as the ability of a heterogeneous catalytic surface to simultaneously chemisorb H and OH species on at least two chemically or structurally different areas of the surface. The section covers theoretical studies of OH chemisorption for well-defined monometallic model systems and reported experimental evidence of the bifunctionality of monometallic surfaces and provides examples of the HOR electrocatalysis on multicomponent materials.

*4.2.1. Theoretical Studies of OH Adsorption in the Framework of the HOR Catalysis.* Theoretical investigations of the adsorption of oxygenated groups on various metallic surfaces have been an important tool for obtaining an improved fundamental understanding of ORR electrocatalysis and the stability of various possible reaction intermediates.[149,150] However, studies of OH adsorption, as an inherent part of the HOR electrocatalysis in basic media, are still relatively scarce. Here we discuss the theoretical investigations of OH adsorption on catalytic surfaces in the framework of the HOR in alkaline media.

Han et al.[151] shed some light on the effect of catalyst particle size with respect to the HOR activity, provided the Volmer or Heyrovsky mechanisms of the reaction. Specifically, the authors studied the effect of Pt particle size and local surface structure on the adsorption of OH. They found that the OH adsorption energy is sensitive to the coordination number and size of the Pt particles, changing by as much as 1 eV in going from an extended Pt(111) surface ("bulk Pt") to the complex surface of a Pt particle with size of 1 nm. Low-coordinated sites on Pt nanoparticles were predicted to adsorb OH more strongly and also showed a stronger sensitivity to the particle size and surface structure than the other sites. For instance, for a 1 nm Pt particle, the bond strength for on-top adsorption of OH varied from −2.61 eV at the center of the (100) facet to −3.35 eV at a vertex of the Pt particle (Figure 19 inset).[151] The authors' conclusions are implicitly supported by DFT calculations.[152] Lin et al.[152] studied several Pt clusters (size range from 3 to 40 atoms) with three different shapes using the DFT approach. The reported results indicate that for all of the clusters, the absolute value of the OH binding energy (OHBE) increases with increasing cluster size. The behavior is summarized in Figure 19, predicting some constant but low values of the OHBE on the surface of large Pt clusters. As the cluster size increases, the average coordination number of surface Pt atoms also increases (lower fraction of edge and kink sites).

Mazher and Al-Odail[153] focused on the Volmer process of the HOR catalysis in alkaline media, as described by the ab initio DFT approach. The investigated system comprised an adsorbent (Tafel's hydrogen preadsorbed monolayer), a metallic Pd(111) surface, and an approaching OH radical. The proximity of a hydroxyl radical to the $H_{ad}$−Pd(111) surface was expected to bring a free energy change as a function of the radical's distance from the surface. A free energy minimum of $\Delta G_H$ = −2.495 eV was calculated for a distance of 3.1 Å between the hydroxyl oxygen and the Pd surface. Water formation was then expected as a next step when this configuration was reached, and some computational evidence supported this idea, with an O−H bond length of 0.978 Å and H−O−H bond angle of 103.6°, similar to those found in a free water molecule. A similar formation of water was predicted at ca. 3.2 Å by Quaino et al.[154]

Balbuena et al.[155] studied the OHBE and preferred adsorption sites of OH for bimetallic or bifunctional Pt clusters, such as PtX, $Pt_2X$, and $PtX_2$ (X = Co, Cr, Ni). The second metal element in the alloy was shown to have a stronger affinity for OH than the Pt sites. Moreover, the authors showed that the second metal could adsorb up to two OH radicals per site. The relative OH adsorption strength on Pt(111) was shown to change with the adsorption mode, decreasing in the following sequence: top > bridge > hollow.[155] Michaelides and Hu[156] used DFT to study the adsorption of hydroxyl radical at


DOI: 10.1021/acscatal.8b00689
ACS Catal. 2018, 8, 6665−6690

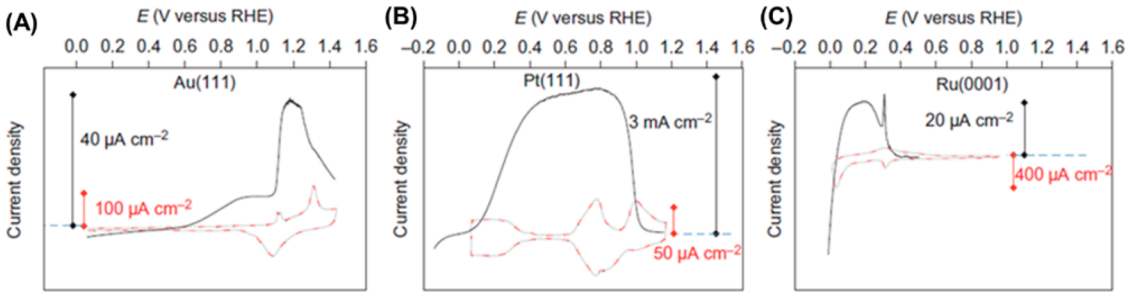


**Figure 20.** HOR polarization curves (black) and CVs (dashed red) for (A) Au(111), (B) Pt(111), and (C) Ru(0001) recorded in 0.1 M KOH. All of the polarization curves were measured at a rotation rate of 1600 rpm. Reprinted with permission from ref 70. Copyright 2013 Springer Nature.

low and high OH coverage and the nature of the intermediate in the formation of water on Pt(111). At low coverage (1/9 to 1/3 monolayer), OH binds preferentially at bridge and top sites with a chemisorption energy of ca. 2.25 eV. At high coverage (1/2 to 1 monolayer), hydrogen bonding between adjacent hydroxyls increases the OH chemisorption energy to ca. 2.5 eV, with a strong preference for on-top OH adsorption, leading to the formation of OH networks. In the work of Elbert et al.,[106] the DFT-calculated adsorption energies of H on Pt(111) and $Pt_3Ru(111)$ were determined to be −0.33 and −0.19 eV, respectively. It was also shown tha, when a Ru site on $Pt_3Ru(111)$ binds $OH_{ad}$, the Pt−$H_{ad}$ bonding is further reduced to −0.12 eV (Table S1). Thus, the authors believed that the incorporation of Ru induces an electronic effect that weakens the Pt−$H_{ad}$ interaction. This likely benefits the oxidative desorption of $H_{ad}$, which was theoretically shown to be the RDS of the HOR in alkaline media.[106]

The selection of studies briefly discussed in this section is far from exhaustive, but the analyses shed some light on the effect played by OH adsorption as the potential intermediate involved in the HOR in alkaline media. The conclusions made in these studies are of high importance for understanding the behavior of OH (co)adsorption on different catalytic surfaces and of the factors determining the surface occupancy by OH.

*4.2.2. Experimental Studies on the Effect of Oxygenated Species on Monometallic Surfaces.* As discussed in the previous sections, it is accepted by many scientists in the field that the HOR in basic media involves two adsorbed species, $H_{ad}$ and $OH_{ad}$. Free adsorption sites are required for both the chemisorption of $H_2$ and the adsorption of OH species. Therefore, it seems reasonable to expect a change in the ability of a surface to catalyze the HOR as a function of its ability to coadsorb oxygenated species in parallel with $H_{ad}$.

A clear illustration of the OH adsorption effect on the HOR kinetics in alkaline media for different facets of Pt was given by Marković et al.[46] Cyclic voltammetry revealed that Pt(111) exhibits separate potential regions for $H_{UPD}$ ($0 < E < 0.4$ V) followed by the double-layer potential region (ca. 0.4 V < $E$ < 0.6 V) and the "butterfly region" ($0.6 < E < 0.9$ V). The butterfly region on Pt(111) is commonly assumed to represent the discharge of $OH^-$ to form a hydroxyl adlayer, while on the Pt(100) and Pt(110) facets $H_{UPD}$ desorption clearly overlaps with OH adsorption (Figure 9).

CO oxidation was used by Marković et al.[46] as an indicator of the presence of oxygen species, since CO oxidation on Pt follows a Langmuir−Hinshelwood surface reaction between the adsorbed CO and oxygen-containing species to form $CO_2$.[157] Electro-oxidation of CO in 0.1 M KOH on Pt(*hkl*) at 2 and 60 °C was studied by Schmidt et al.[98] as an indicator of the presence of $OH_{ad}$ on the surface. Because the onset for CO oxidation on Pt(111) was observed in the $H_{UPD}$ potential region, it was proposed that $OH_{ad}$ is coadsorbed with $H_{UPD}$. OH adsorbs selectively at defect sites with a Pt−$OH_{ad}$ bond energy of ca. 206−216 kJ $mol^{-1}$, which can be compared with the Pt−OH bond energy of ca. 136 kJ $mol^{-1}$ in the "butterfly region". Thus, the catalytic activity of Pt facets in the $H_{UPD}$ potential region implies that in alkaline solution, $OH_{ad}$ is adsorbed at potentials below ca. 0.2 V. On Pt(100), the dissociative adsorption of $H_2$ molecules was shown to be inhibited even at low surface coverage by $OH_{ad}$.[46] The relationship of the kinetic current density ($i_k$), determined from the $y$ intercept of the Levich−Koutecky plot, and the surface coverage ($\theta$), obtained from the adsorption isotherm of $OH_{ad}$, was plotted in the form of log $i_k$ versus $\log(1-\theta)$. The resulting relationship was found to be linear with a slope of 2.[46] This implies that the current density of the HOR on Pt(100) in the $OH_{ad}$ region decreases as the second power, i.e., unoccupied Pt pair sites are required for the dissociative chemisorption of $H_2$.

Direct experimental evidence of the OH coadsorption effect on the HOR electrocatalysis on a broad range of catalytic materials was reported by Strmcnik et al.[70] A series of catalytic materials including Au, Ru, Pt, and Ir having different affinities for H and OH were investigated in regard to the HOR in 0.1 M KOH (Figure 20).[70] The HOR on Au(111) in alkaline solutions occurs above 0.6 V vs RHE, coinciding with the adsorption of $OH_{ad}$: the onset observed above 0.6 V is followed by an increase in the oxidation current at 1.1 V and a rapid decrease in activity above 1.3 V. For Ir, on the basis of a CO displacement experiment,[158] it was shown that hydrogen adsorption/desorption on Ir is also accompanied by $OH_{ad}$ desorption/adsorption. This is believed to be the main reason for the 25-fold higher HOR activity at 0.05 V for Ir(111) compared with Pt(111). For Pt, Strmcnik et al.[70] reported that the HOR activity is sensitive to the catalyst structure in alkaline solutions, mainly because of the stronger $OH_{ad}$ adsorption on low-coordinated Pt atoms versus highly coordinated Pt sites. This hypothesis is in good agreement with the theoretical studies discussed in section 4.2.1. To further support the hypothesis, the number of low-coordinated sites on Pt(111) terraces was either decreased by using a CO annealing protocol or increased by depositing Pt adislands. As expected, the HOR was strongly inhibited on the former surface, while it was activated on the latter.

No inhibition of the HOR by surface oxygenated species was observed on Pt(110), which has more coordinatively unsaturated Pt atoms and also higher HOR activity than



DOI: 10.1021/acscatal.8b00689
ACS Catal. 2018, 8, 6665−6690

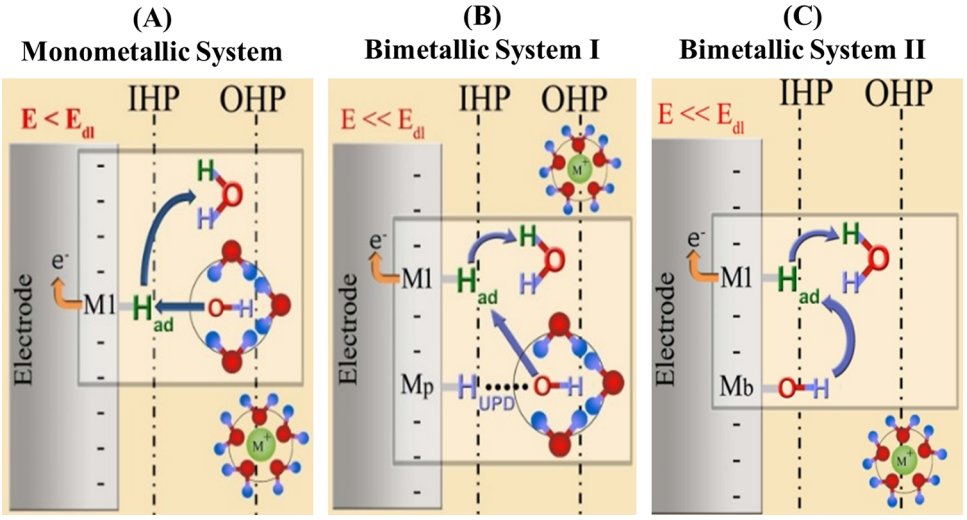


**Figure 21.** Relationship between the HOR electrocatalysis and electrochemical double-layer structure. Reprinted with permission from ref 160. Copyright 2017 Elsevier.

Pt(111) and Pt(100) despite a larger coverage by oxygenated species on Pt(110).[108]

The experimental data provided by Marković and co-workers[46,108] and Strmcnik et al.[70] for the HOR in alkaline media for monometallic surfaces serve as a clear example of bifunctional catalysis taking place on active centers that, while based on the same metal, are energetically different.

On the basis of these experimental observations, it was concluded that fine-tuning of the OH adsorption energy offers a promising pathway for the design of more efficient anode catalysts in basic media. The mainstream approach to realize this tuning is to develop bimetallic materials that provide chemically different active sites for the dissociative adsorption of $H_2$ and adsorption of reactive $OH_{ad}$, as discussed in the next subsection.

*4.2.3. Experimental Studies on Bifunctional HOR Catalysts Designed with Several Metals.* In order to compare the oxophilicities of Pt/C and PtRu/C in alkaline media and to show that the oxophilicity of the surface plays a crucial role, Wang et al.[6] employed CO stripping as a probe experiment. The results evidenced that reactive hydroxyl species can be generated on certain sites of the Pt surface at more negative potentials (onset of CO stripping at ca. 0.2 V) than on the PtRu surface (onset of CO stripping at ca. 0.35 V). Therefore, the authors concluded that the enhancement in the kinetics of the HOR catalyzed by PtRu/C can hardly be ascribed to an oxophilic effect but rather is due to weakening of the Pt−$H_{ad}$ interaction.[6] More explicit examples of bifunctional catalysis are provided by Strmcnik et al.,[70] Alesker et al.,[18] and Miller and co-workers.[22,23] A $Pt_{0.1}Ru_{0.9}$ catalyst was investigated in the HOR in 0.1 M KOH by Strmcnik et al.[70] The authors showed that the activity of the $Pt_{0.1}Ru_{0.9}$ catalyst in alkaline solution can be more than 5-fold higher than that of state-of-the-art platinum catalysts. It was proposed that $Pt_{0.1}Ru_{0.9}$ has an optimal balance between the active sites that are required for the adsorption/dissociation of $H_2$ and for the adsorption of hydroxyl species.[70] The more oxophilic sites in PtRu catalysts (i.e., Ru oxophilic atoms) are assumed to facilitate the adsorption of $OH_{ad}$ species. Those in turn react with the hydrogen intermediates ($H_{ad}$) that are adsorbed on the less oxophilic noble surface sites (e.g., Pt).

Another type of bimetallic catalyst, namely, Pd/Ni, was synthesized and investigated by Alesker et al.[18] The contact between Pd and Ni nanoislands was proved to significantly enhance the activity of the Pd catalyst, as evidenced by a negative shift of ca. 0.2 V in the HOR onset potential compared with the case of a Pd-only catalyst. The high activity of this Pd/Ni nanocomposite was assigned to the presence of $OH_{ad}$ species, or bifunctional catalysis, on the surface of the oxophilic Ni (Figure 6B), although no direct experimental evidence was provided. Bakos et al.[71] demonstrated that a Pd coverage as low as 1.5% on Ni nanoparticles is sufficient to provide bifunctional catalysis at a high current density (0.57 mA $cm^{-2}_{Pd}$ at an overvoltage of 0.05 V; Table S3) compared with pure Ni. The current density increases linearly with the Pd coverage up to a Pd coverage of 17%. Upon further increases in the Pd coverage, the current density reaches a plateau. The comparison with Pd supported on carbon shows the clear benefit of the bimetallic catalyst, the latter having an $i_0$ value of ca. 1 mA $cm^{-2}_{Pd}$ for 1.5% Pd/Ni in 0.1 M KOH (Table S2). Significant progress in non-PGM AEMFC performance (section 5) was recently made through the development of $CeO_2$-decorated carbon-supported nanoparticles by Miller and co-workers.[22,23] The authors ascribe the catalytic effect to bifunctional catalysis between Pd and the oxophilic ceria (Figure 6A), although oxide-supported catalysts are widely known for their hydrogen-spillover properties,[159] which could play a role in the HOR electrocatalysis as well.

Very recently, Ramaswamy et al.[160] proposed a heretofore unknown modern rendition of the double-layer structure wherein specifically adsorbed (M−$OH_{ad}$) and quasi-specifically adsorbed (M−$H_{ad/UPD}$−$OH_{q\text{-}ad}$) reactive hydroxide species described appropriately the $H_2$ oxidation kinetics at high pH on monometallic as well as bimetallic catalyst surfaces. Here $OH_{ad}$ refers to the specifically adsorbed reactive species localized in the inner Helmholtz plane and $OH_{q\text{-}ad}$ refers to the quasi-specifically adsorbed reactive species localized in the outer Helmholtz plane. According to this rendition, it was proposed that the fundamental limitation in the alkaline HOR process is closely related to the ability to bring a negatively charged hydroxide anion to the plane of closest approach of the negatively charged electrode surface (eq 20):



DOI: 10.1021/acscatal.8b00689
ACS Catal. 2018, 8, 6665−6690

$$Pt + H_{ad} + OH^- \rightarrow Pt + H_2O \quad (20)$$

Ramaswamy's work[160] provides experimental evidence highlighting the need to distinguish the concepts of HBE (applicable only for predicting the reaction rate close to equilibrium) and the HOR catalysis in general (including also the reaction far from equilibrium).

On a monometallic Pt surface, the higher overpotential required for the HOR on Pt in alkaline electrolytes was suggested to be due to the higher activation energy required to reach an exclusive transition state structure of the form Pt−$H_{ad}$−$OH_{q\text{-}ad}$, which is not involved under acidic conditions. This transition state structure requires a higher activation energy since it involves the approach of a negatively charged anion ($OH^-$) to the plane of closest approach (i.e., the outer Helmholtz plane in the double layer) to form the quasi-adsorbed species $OH_{q\text{-}ad}$. It was proposed that the HOR overpotential can be reduced by alloying a primary active site capable of dissociatively adsorbing $H_2$ (e.g., Pt) with either (i) a base transition metal ($M_b$) that is passivated with a (hydr)oxide layer ($M_b$−$OH_{ad}$) at potentials low enough in the HOR region or (ii) a metal, typically from a precious metal group ($M_p$) that can activate one-electron reduction of water to form $M_p$−$H_{ad/UPD}$−$OH_{q\text{-}ad}$ clusters. In such bimetallic systems, the Pt−$H_{ad}$ intermediate reacts either with the $OH_{ad}$ species formed on an adjacent base metal ($M_b$−$OH_{ad}$) in the former case or with the $OH_{q\text{-}ad}$ species formed on the precious metal alloying element ($M_p$−$H_{UPD}$−$OH_{q\text{-}ad}$) in the latter case to enhance the HOR kinetics (Figure 21).

The generic reaction mechanism proposed for the HOR in dilute alkaline electrolytes on mono- and bimetallic catalyst systems is the following. M1 represents a metal site capable of dissociatively adsorbing molecular hydrogen. In Figure 21B, the alloying element $M_p$ represents a precious metal site capable of forming $H_{UPD}$ in the alkaline electrolyte. In Figure 21C, the alloying element $M_b$ represents a base metal site passivated with adsorbed (hydr)oxide species in dilute alkaline electrolytes.

The synergetic effect observed for the multicomponent/multiphase electrocatalysts in the HOR, as opposed to unmodified monometallic catalysts, still needs to be proven via direct experimental data revealing the functionalities of the components. This is more relevant for new composite materials like Pd@$CeO_2$, Pd@Ni, etc. discussed hitherto, since Pt@Ru alloys can be considered as a conventional example of bifunctional catalysis in the field of electrochemistry. Theoretical predictions for such multicomponent and multiphase systems are complicated, and therefore, vast experimental screening of a material library is needed in order to shed some light on the phenomenon of bifunctional electrocatalysis for the HOR in alkaline media.

## 5. CHALLENGES IN THE IMPLEMENTATION OF THE HOR ELECTROCATALYSTS IN AEMFCS

The results discussed in this work have aimed to summarize the fundamental knowledge on the HOR electrocatalysis in basic media. Eventually, such electrocatalysts are intended to be used on the anode of $H_2$−air AEMFCs. Therefore, the properties of the HOR catalysts have to meet specific requirements to sustain the working conditions of AEMFC anodes. The conditions include elevated temperatures (possibly up to 95 °C in the future, when developed AEMs will resist such temperatures); high pH values of 11−14 (simulating the conditions in the anion conducting ionomers and membrane); changing relative humidity (from the highly humid water-generating anode to the dry and hydroxyl-microsolvated cathode); the possible presence of trace $O_2$ while the AEMFC is idle or during the start/shutdown cycles, with possible associated high anode potential if the anode catalyst also shows some ORR activity; possible poisoning upon contact with the AEI and AEM (functional groups, trace amount of halogen cations remaining from ionomer production). This section summarizes key observations on the performance of AEMFCs to date, explores how these experimental observations can be linked to the fundamental development of the HOR catalyst surface, and identifies some important concepts for successful implementation of catalysts with high HOR activities in liquid electrolytes as highly active AEMFC anodes where the interface is catalyst−AEI.

**5.1. Beginning-of-Life Performance of Pt/Pt AEMFCs.** Currently there are around 150 studies reporting AEMFC performance, as recently summarized by Dekel[3] and Gottesfeld et al.[161] Among them, most anode catalysts are Pt-based (Table S4).[4,6,7,9−11] An analysis of the AEMFC literature shows that the highest cell performances were registered for MEAs containing a PtRu catalyst on the anode side.[4,6,7,9,10] It was shown that PtRu alloys have an exchange current density 2 to 6 times higher than that of Pt,[70] as previously shown in liquid electrolyte studies (see section 4 and Table S2). Recently, through proper water management and electrode design, the possibility of reaching high BoL performances of AEMFCs was shown with Pt- and PtRu-based catalysts on the cathode and anode, respectively (see Table S4). Usual Pt loadings at the anode are 0.4−1 mg $cm^{-2}$, and the Pt content supported on carbon spans between 20 and 100% (platinum black). The most common ionomer loadings in the catalytic layer are 20−30%, but the chemical nature of the ionomers and the way they are mixed with the catalyst vary from study to study.

**5.2. Beginning-of-Life Performance of Pt-Free AEMFCs.** Only a very few works on Pt-free AEMFCs are documented.[18−23] Some more detailed information on Pt-free AEMFCs is provided in Table S5, which is supplementary to Figure 11 in Dekel's recently published review.[3] A high peak power density of 500 mW $cm^{-2}$ was reached for Pd/C−$CeO_2$ (10% Pd) at 73 °C with a dry anode and fully humidified cathode.[22] Lower power densities of 460 and 390 mW $cm^{-2}$ were obtained with Pd/C−$CeO_2$ (20% Pd) and Pd/C−$CeO_2$ (6% Pd), respectively, as the anode catalyst.[23] Much lower performance has been observed for PGM-free AEMFCs. Currently, a maximum power density of 76 mW $cm^{-2}$ was reached with partially passivated Ni nanoparticles on the anode and Ag nanoparticles on the cathode.[20] Rather high loadings of silver or silver alloys are utilized on the cathode (up to 3 mg $cm^{-2}$). The loadings of Ni-based catalysts are even higher (5−17.5 mg $cm^{-2}_{Ni}$). Lu et al.[20] have claimed that there was no degradation of their AEMFC with NiCr/C as the anode for ca. 100 h of operation. The longevity of Ni-based anodes is limited by the catalyst chemical and electrochemical passivation in the AEMFC, as opposed to traditional liquid-electrolyte-based alkaline fuel cells (AFCs) with highly concentrated alkaline solutions (e.g., 30%). Wagner et al.[162] and Gülzow et al.[163] have demonstrated nickel anodes to exhibit a 5000 h level or even higher catalyst durability in liquid-electrolyte-based AFCs. The relatively small anode losses reported for Ni catalysts in liquid circulating alkaline fuel cells[131,135,164] could not be reproduced for AEMFC anodes using Ni or other PGM-free catalysts.



DOI: 10.1021/acscatal.8b00689
ACS Catal. 2018, 8, 6665−6690

Lu et al.[20] have shown that the Ni catalysts commonly used in AFCs do not work well in AEMFCs. It was found that the hydrogen anodes made from such Ni catalysts show an electrode potential characteristic of nickel oxides instead of the potential of a hydrogen electrode. The electrolysis method used in AFCs to activate the Ni anode in a separate electrolyzer[139] is unfortunately inapplicable for AEMFCs using a MEA structure unless a bifunctional oxygen electrode can be found.

Villarrubia et al.[165] investigated the behavior of nonprecious Ni-based catalysts in the presence of quaternary-ammonium-functionalized ionomers and showed that the time-dependent cationic group adsorption is less than that for a Pt catalyst. These studies suggest that organic cation chemisorption and the resultant inevitable Pt surface layer change could be a major issue responsible for the low AEMFC performance and durability. However, no significant effect of cationic groups on the HOR kinetics of non-PGM catalysts has been observed.

**5.3. Anion-Exchange Ionomer−HOR Electrocatalyst Interface.** Studies of the interface between AEIs and HOR electrocatalysts are still in their infancy. To date there have been only a few studies reporting the effect of different AEIs and cationic groups on Pt catalytic properties. Those few studies nevertheless all clearly show the poisoning of Pt by the anion ionomer. Yim et al.[166] showed that in 0.1 M 1,1,3,3-tetramethylguanidine and benzyltrimethylammonium hydroxide solutions, the HOR activity of Pt is limited by adsorption of the cationic group. The cation adsorption results in a rapid activity decrease, from which the authors hypothesized that this could be one of the reasons for AEMFC performance degradation. In the same study,[166] the authors also investigated the HOR at the Pt−AEI interface using two different AEIs, benzyltrimethylammonium-tethered poly(phenylene) (ATM-PP) and a phenylpentamethylguanidinium-tethered perfluorinated polymer (M-Nafion-FA-TMG). Substantial inhibition of the HOR was shown for the Pt−ATM-PP interface due to the possible cationic group adsorption, whereas the reaction was virtually unaffected at the Pt−M-Nafion-FA-TMG interface. Chung and co-workers[167,168] showed that the HOR of Pt in 0.1 M tetramethylammonium hydroxide solution is adversely impacted by time-dependent and potential-driven cation−hydroxide−water coadsorption. Impedance analysis suggested that the HOR inhibition is mainly caused by the hydrogen diffusion barrier of the coadsorbed trilayer rather than intuitive catalyst site blocking by the adsorbed cation species.[167] Matanovic et al.[169] compared the HOR with carbon-supported Pt in 0.1 M tetramethylammonium hydroxide and benzyltrimethylammonium hydroxide solutions to study the possible effect of benzene adsorption on the HOR activity under alkaline conditions. The HOR activity of Pt was shown to be inhibited by benzene adsorption, while bimetallic catalysts such as PtMo/C, PtNi/C, and PtRu/C can reduce the adsorption of benzene and thereby improve the HOR activity.

Finally, as a brief summary of this section, we would like to emphasize that significant progress has already been made in the understanding of water management in AEMFCs with Pt-based and especially PtRu-based electrodes. Water transport was identified as one of the most limiting parameters, and its management resulted in high current densities above 3 A $cm^{-2}$ and peak power densities of 0.6−1.5 W $cm^{-2}$. Even though Pt-free AEMFCs underperform those cells based on Pt catalysts (Table S5), the recently achieved performance of 0.12 W $cm^{-2}$ with NiMo anode catalysts shows that PGM catalysts might be replaced by PGM-free catalysts at both electrodes of AEMFCs in the near future. Studies of the specific chemical and physical interactions between the catalyst surface and anion-exchange ionomers/ion-exchange membranes should be particularly mentioned as an understudied aspect of MEA design in AEMFCs.

## 6. CONCLUSIONS

From a thermodynamic viewpoint, AEMFC technology opens up possibilities for using a broad class of PGM-free materials to catalyze the electrochemical reactions in low-temperature polymer electrolyte fuel cells, which is highly promising to solve the cost barriers of the mature PEMFC counterpart. It is well-recognized, however, that the competitive interest of AEMFCs versus PEMFCs hinges on the further development of (i) highly active and affordable PGM-free catalysts and (ii) more stable AEM and AEI materials. The former task is mainly challenged by the sluggish kinetics of the HOR in alkaline media, even for PGM-based electrocatalysts. Thus, the energy conversion efficiency and power density of AEMFCs are limited not only by the ORR kinetics, as was known before, but also by the HOR kinetics, especially when moving to PGM-free catalysts. In this review, we have shown that all non-PGM catalysts that are currently known to catalyze the HOR comprise nickel, often alloyed with a one or more non-PGM metals. However, the HOR mechanisms of such materials are still poorly understood, and the progress in their synthesis is restricted because of the trial-and-error approach. Our review embraces both state-of-the-art experimental and theoretical studies on the HOR electrocatalysis in basic media. We have critically discussed the most recent electrocatalyst design approaches, which are mainly based on the following:

(1) The hypothesized HOR mechanisms, assuming one of the following steps to be rate-determining: (A) dissociative adsorption of molecular dihydrogen, (B) electron transfer from molecular dihydrogen to the catalyst, and (C) discharge of the adsorbed hydrogen atom.
(2) The widely discussed "HBE theory" considering $H_2$ dissociation as the HOR bottleneck and mostly dealing with theoretical investigations.
(3) The disputable "$H_{UPD}$ concept" assuming $H_{UPD}$ species to be the HOR intermediate.
(4) The "bifunctional theory" implying the key role of the multifunctional catalytic surface which provides sites for adsorption of H and OH species. In contrast to the HOR in acidic media, where all of the accessible active sites are solely destined to chemisorb hydrogen atoms, in alkaline media the catalytic surface has to provide active sites for the coadsorption of hydrogen atoms as well as adsorbed hydroxide species.

Since each subsection of this review includes specific subconclusions, those are not repeated here. Instead, we outline here possible directions for future investigations based on the current scientific background existing in the field, which this review has attempted to summarize. Even though significant progress has been achieved lately in understanding the main factors restricting the performance of AEMFCs with Pt(PGM)-based electrodes and high beginning-of-life peak power density values of above 1 W $cm^{-2}$, the precious metal catalyst loadings on the anode are quite high (up to 0.6 mg $cm^{-2}$). This motivates the development of ultralow-PGM catalysts and scale-up of the synthetic methods. Even though


DOI: 10.1021/acscatal.8b00689
ACS Catal. 2018, 8, 6665−6690

state-of-the-art non-PGM AEMFCs underperform those based on Pt catalysts, the recently achieved performance of Ni-based anode catalysts demonstrates the potential for PGM-free AEMFC cathodes and anodes. Thus, non-PGM HOR electrocatalysis is a promising field of research. In our opinion, the following challenging tasks are important to further advance the knowledge in the HOR electrocatalysis in alkaline media:

1. Experimental studies focusing on the alleged bifunctional effect in the HOR catalysis for improved multicomponent electrocatalysts and better theoretical understanding of the fine-tuning balance between H and OH coadsorption along with electron transfer processes.
2. Systematic studies to investigate the effect of modifying Ni, mostly with transition metals, on its electrocatalytic activity.
3. Exploration of novel non-PGM and non-Ni electrocatalytic materials with high affinity for hydrogen chemisorption.
4. Development of new approaches to decrease surface oxidation or OH coverage at moderate overpotentials.
5. Stability studies on the HOR electrocatalysts, including load cycling, operando analysis of the metal leaching rate, and the effects of startup/shutdown and the presence of air in the anode compartment.
6. Improved understanding of the interactions between anion-exchange ionomers and various electrocatalysts.

Advances in the above-mentioned challenges will help replacing PGM catalysts with non-PGM catalysts at the anode in the future, thereby strongly contributing to the establishment of AEMFC technology as a genuine alternative to PEMFCs.

## ■ ASSOCIATED CONTENT

### Supporting Information

The Supporting Information is available free of charge on the ACS Publications website at DOI: 10.1021/acscatal.8b00689.

Table S1. Summary of theoretical and experimental values of HBE, metal−hydrogen bond energy and free energy of hydrogen adsorption, and energy of the d-band center for a variety of catalytic materials, as reported in the literature. Table S2. Exchange current density, mass specific activity, and activation energy values for the HOR in basic electrolytes on different electrocatalytic materials. Table S3. Specific activity and mass specific activity values at polarizations of 0.05 and 0.1 V for the HOR in basic electrolytes on different electrocatalytic materials. Table S4. Beginning-of-life performance of Pt/Pt-based state-of-the-art AEMFCs, brief MEA fabrication procedures, fuel cell test conditions, peak power densities in W $cm^{-2}$ and corresponding current densities in mA $cm^{-2}$, and current densities in mA $cm^{-2}$ at cell voltages of 0.85 and 0.6 V. Table S5. Beginning-of-life performance of Pt-free state-of-the-art AEMFCs, brief MEA fabrication procedures, and the fuel cell test conditions (PDF)

## ■ AUTHOR INFORMATION


### Corresponding Authors

*Elena S. Davydova e-mail: elena.s.davydova@gmail.com.
*Dario R. Dekel e-mail: dario@technion.ac.il.

### ORCID

Dario R. Dekel: 0000-0002-8610-0808


### Notes

The authors declare no competing financial interest.

## ■ ACKNOWLEDGMENTS

This work was partially funded by the European Union's Horizon 2020 Research and Innovation Program under Grant Agreement 721065 (Project CREATE); by the Grand Technion Energy Program (GTEP); by the Ministry of Science, Technology and Space of Israel through the M.era-NET Transnational Call 2015, NEXTGAME Project (Grant 3-12940), through the Israel−Germany Batteries Collaboration Call 2017 (German Grant 2675), and through Grant 3-12948; by the Russell Berrie Nanotechnology Institute, Technion; by the 2nd Israel National Research Center for Electrochemical Propulsion (INREP2-ISF); by the Ministry of National Infrastructure, Energy and Water Resources of Israel (Grant 3-13671); and by the Israel Science Foundation (ISF) (Grant 1481/17).

## ■ REFERENCES


(1) Varcoe, J. R.; Atanassov, P.; Dekel, D. R.; Herring, A. M.; Hickner, M. A.; Kohl, P. A.; Kucernak, A. R.; Mustain, W. E.; Nijmeijer, K.; Scott, K.; Xu, T.; Zhuang, L. Anion-Exchange Membranes in Electrochemical Energy Systems. *Energy Environ. Sci.* **2014**, *7*, 3135−3191.

(2) Varcoe, J. R.; Slade, R. C. T. Prospects for Alkaline Anion-Exchange Membranes in Low Temperature Fuel Cells. *Fuel Cells* **2005**, *5*, 187−200.

(3) Dekel, D. R. Review of Cell Performance in Anion Exchange Membrane Fuel Cells. *J. Power Sources* **2018**, *375*, 158−169.

(4) Mamlouk, M.; Horsfall, J. A.; Williams, C.; Scott, K. Radiation Grafted Membranes for Superior Anion Exchange Polymer Membrane Fuel Cells Performance. *Int. J. Hydrogen Energy* **2012**, *37*, 11912−11920.

(5) Mamlouk, M.; Scott, K.; Horsfall, J. A.; Williams, C. The Effect of Electrode Parameters on the Performance of Anion Exchange Polymer Membrane Fuel Cells. *Int. J. Hydrogen Energy* **2011**, *36*, 7191−7198.

(6) Wang, Y.; Wang, G.; Li, G.; Huang, B.; Pan, J.; Liu, Q.; Han, J.; Xiao, L.; Lu, J.; Zhuang, L. Pt−Ru Catalyzed Hydrogen Oxidation in Alkaline Media: Oxophilic Effect or Electronic Effect? *Energy Environ. Sci.* **2015**, *8*, 177−181.

(7) Kaspar, R. B.; Letterio, M. P.; Wittkopf, J. A.; Gong, K.; Gu, S.; Yan, Y. Manipulating Water in High-Performance Hydroxide Exchange Membrane Fuel Cells through Asymmetric Humidification and Wetproofing. *J. Electrochem. Soc.* **2015**, *162*, F483−F488.

(8) Li, G.; Wang, Y.; Pan, J.; Han, J.; Liu, Q.; Li, X.; Li, P.; Chen, C.; Xiao, L.; Lu, J.; Zhuang, L. Carbonation Effects on the Performance of Alkaline Polymer Electrolyte Fuel Cells. *Int. J. Hydrogen Energy* **2015**, *40*, 6655−6660.

(9) Ponce-González, J.; Whelligan, D. K.; Wang, L.; Bance-Soualhi, R.; Wang, Y.; Peng, Y.; Peng, H.; Apperley, D. C.; Sarode, H. N.; Pandey, T. P.; Divekar, A. G.; Seifert, S.; Herring, A. M.; Zhuang, L.; Varcoe, J. R. High Performance Aliphatic-Heterocyclic Benzyl-Quaternary Ammonium Radiation-Grafted Anion-Exchange Membranes. *Energy Environ. Sci.* **2016**, *9*, 3724−3735.

(10) Wang, L.; Magliocca, E.; Cunningham, E. L.; Mustain, W. E.; Poynton, S. D.; Escudero-Cid, R.; Nasef, M. M.; Ponce-González, J.; Bance-Souahli, R.; Slade, R. C. T.; Whelligan, D. K.; Varcoe, J. R. An Optimised Synthesis of High Performance Radiation-Grafted Anion-Exchange Membranes. *Green Chem.* **2017**, *19*, 831−843.

(11) Omasta, T. J.; Wang, L.; Peng, X.; Lewis, C. A.; Varcoe, J. R.; Mustain, W. E. Importance of Balancing Membrane and Electrode Water in Anion Exchange Membrane Fuel Cells. *J. Power Sources* **2018**, *375*, 205−213.

(12) Wang, C.-H.; Yang, C.-W.; Lin, Y.-C.; Chang, S.-T.; Chang, S. L. Y. Cobalt−iron(II,III) Oxide Hybrid Catalysis with Enhanced




DOI: 10.1021/acscatal.8b00689
*ACS Catal.* 2018, 8, 6665−6690

Catalytic Activities for Oxygen Reduction in Anion Exchange Membrane Fuel Cell. *J. Power Sources* **2015**, *277*, 147−154.
(13) Li, X.; Popov, B. N.; Kawahara, T.; Yanagi, H. Non-Precious Metal Catalysts Synthesized from Precursors of Carbon, Nitrogen, and Transition Metal for Oxygen Reduction in Alkaline Fuel Cells. *J. Power Sources* **2011**, *196*, 1717−1722.
(14) Tarasevich, M. R.; Davydova, E. S. Nonplatinum Cathodic Catalysts for Fuel Cells with Alkaline Electrolyte (Review). *Russ. J. Electrochem.* **2016**, *52*, 193−219.
(15) Saito, M.; Takakuwa, T.; Kenko, T.; Daimon, H.; Tasaka, A.; Inaba, M.; Shiroishi, H.; Hatai, T.; Kuwano, J. New Oxygen Reduction Electrocatalysts Based on Lanthanum Manganite Oxides and Their Application to the Cathode of AEMFCs. *ECS Trans.* **2013**, *58*, 1335−1345.
(16) Kruusenberg, I.; Matisen, L.; Shah, Q.; Kannan, A. M.; Tammeveski, K. Non-Platinum Cathode Catalysts for Alkaline Membrane Fuel Cells. *Int. J. Hydrogen Energy* **2012**, *37*, 4406−4412.
(17) Mamlouk, M.; Kumar, S. M. S.; Gouerec, P.; Scott, K. Electrochemical and Fuel Cell Evaluation of Co Based Catalyst for Oxygen Reduction in Anion Exchange Polymer Membrane Fuel Cells. *J. Power Sources* **2011**, *196*, 7594−7600.
(18) Alesker, M.; Page, M.; Shviro, M.; Paska, Y.; Gershinsky, G.; Dekel, D. R.; Zitoun, D. Palladium/nickel Bifunctional Electrocatalyst for Hydrogen Oxidation Reaction in Alkaline Membrane Fuel Cell. *J. Power Sources* **2016**, *304*, 332−339.
(19) Gu, S.; Sheng, W.; Cai, R.; Alia, S. M.; Song, S.; Jensen, K. O.; Yan, Y. An Efficient Ag−ionomer Interface for Hydroxide Exchange Membrane Fuel Cells. *Chem. Commun.* **2013**, *49*, 131−133.
(20) Lu, S. F.; Pan, J.; Huang, A. B.; Zhuang, L.; Lu, J. T. Alkaline Polymer Electrolyte Fuel Cells Completely Free from Noble Metal Catalysts. *Proc. Natl. Acad. Sci. U. S. A.* **2008**, *105*, 20611−20614.
(21) Hu, Q.; Li, G.; Pan, J.; Tan, L.; Lu, J.; Zhuang, L. Alkaline Polymer Electrolyte Fuel Cell with Ni-Based Anode and Co-Based Cathode. *Int. J. Hydrogen Energy* **2013**, *38*, 16264−16268.
(22) Miller, H. A.; Lavacchi, A.; Vizza, F.; Marelli, M.; Di Benedetto, F.; D'Acapito, F.; Paska, Y.; Page, M.; Dekel, D. R. A Pd/C−$CeO_2$ Anode Catalyst for High-Performance Platinum-Free Anion Exchange Membrane Fuel Cells. *Angew. Chem., Int. Ed.* **2016**, *55*, 6004−6007.
(23) Miller, H. A.; Vizza, F.; Marelli, M.; Zadick, A.; Dubau, L.; Chatenet, M.; Geiger, S.; Cherevko, S.; Doan, H.; Pavlicek, R. K.; Mukerjee, S.; Dekel, D. R. Highly Active Nanostructured Palladium-Ceria Electrocatalysts for the Hydrogen Oxidation Reaction in Alkaline Medium. *Nano Energy* **2017**, *33*, 293−305.
(24) Serov, A. *Development of PGM-Free Catalysts for Hydrogen Oxidation Reaction in Alkaline Media*, 2016.
(25) Serov, A. *Development of PGM-Free Catalysts for Hydrogen Oxidation Reaction in Alkaline Media*, 2017.
(26) Serov, A.; Artyushkova, K.; Niangar, E.; Wang, C.; Dale, N.; Jaouen, F.; Sougrati, M. T.; Jia, Q.; Mukerjee, S.; Atanassov, P. Nano-Structured Non-Platinum Catalysts for Automotive Fuel Cell Application. *Nano Energy* **2015**, *16*, 293−300.
(27) Chen, Y.; Gokhale, R.; Serov, A.; Artyushkova, K.; Atanassov, P. Novel Highly Active and Selective Fe-N-C Oxygen Reduction Electrocatalysts Derived from in-Situ Polymerization Pyrolysis. *Nano Energy* **2017**, *38*, 201−209.
(28) Gokhale, R.; Chen, Y.; Serov, A.; Artyushkova, K.; Atanassov, P. Direct Synthesis of Platinum Group Metal-Free Fe-N-C Catalyst for Oxygen Reduction Reaction in Alkaline Media. *Electrochem. Commun.* **2016**, *72*, 140−143.
(29) Wu, G.; Zelenay, P. Nanostructured Nonprecious Metal Catalysts for Oxygen Reduction Reaction. *Acc. Chem. Res.* **2013**, *46*, 1878−1889.
(30) Zhutaeva, G. V.; Bogdanovskaya, V. A.; Davydova, E. S.; Kazanskii, L. P.; Tarasevich, M. R. Kinetics and Mechanism of Oxygen Electroreduction on Vulcan XC72R Carbon Black Modified by Pyrolysis Products of Cobalt 5,10,15,20-tetrakis(4- Methoxyphenyl)-porphyrine in a Broad pH Interval. *J. Solid State Electrochem.* **2014**, *18*, 1319−1334.
(31) Gasteiger, H. A.; Kocha, S. S.; Sompalli, B.; Wagner, F. T. Activity Benchmarks and Requirements for Pt, Pt-Alloy, and Non-Pt Oxygen Reduction Catalysts for PEMFCs. *Appl. Catal., B* **2005**, *56*, 9−36.
(32) Markovic, N.; Gasteiger, H.; Ross, P. N., Jr. Kinetics of Oxygen Reduction on Pt(hkl) Electrodes: Implications for the Crystallite Size Effect with Supported Pt Electrocatalysts. *J. Electrochem. Soc.* **1997**, *144*, 1591−1597.
(33) Meng, H.; Jaouen, F.; Proietti, E.; Lefèvre, M.; Dodelet, J.-P. pH-Effect on Oxygen Reduction Activity of Fe-Based Electro-Catalysts. *Electrochem. Commun.* **2009**, *11*, 1986−1989.
(34) Demarconnay, L.; Coutanceau, C.; Léger, J. M. Electroreduction of Dioxygen (ORR) in Alkaline Medium on Ag/C and Pt/C Nanostructured Catalysts - Effect of the Presence of Methanol. *Electrochim. Acta* **2004**, *49*, 4513−4521.
(35) Du, J.; Chen, C.; Cheng, F.; Chen, J. Rapid Synthesis and Efficient Electrocatalytic Oxygen Reduction/evolution Reaction of $CoMn_2O_4$ Nanodots Supported on Graphene. *Inorg. Chem.* **2015**, *54*, 5467−5474.
(36) Li, C.; Han, X.; Cheng, F.; Hu, Y.; Chen, C.; Chen, J. Phase and Composition Controllable Synthesis of Cobalt Manganese Spinel Nanoparticles towards Efficient Oxygen Electrocatalysis. *Nat. Commun.* **2015**, *6*, 7345.
(37) Meng, Y.; Song, W.; Huang, H.; Ren, Z.; Chen, S.-Y.; Suib, S. L. Structure−Property Relationship of Bifunctional $MnO_2$ Nanostructures: Highly Efficient, Ultra-Stable Electrochemical Water Oxidation and Oxygen Reduction Reaction Catalysts Identified in Alkaline Media. *J. Am. Chem. Soc.* **2014**, *136*, 11452−11464.
(38) Sheng, W.; Gasteiger, H. A.; Shao-Horn, Y. Hydrogen Oxidation and Evolution Reaction Kinetics on Platinum: Acid vs Alkaline Electrolytes. *J. Electrochem. Soc.* **2010**, *157*, B1529−B1536.
(39) Zheng, J.; Sheng, W.; Zhuang, Z.; Xu, B.; Yan, Y. Universal Dependence of Hydrogen Oxidation and Evolution Reaction Activity of Platinum-Group Metals on pH and Hydrogen Binding Energy. *Sci. Adv.* **2016**, *2*, e1501602.
(40) Mahoney, E. G.; Sheng, W.; Yan, Y.; Chen, J. G. Platinum-Modified Gold Electrocatalysts for the Hydrogen Oxidation Reaction in Alkaline Electrolytes. *ChemElectroChem* **2014**, *1*, 2058−2063.
(41) Alia, S. M.; Pivovar, B. S.; Yan, Y. Platinum Coated Copper Nanowires with High Activity for Hydrogen Oxidation Reaction in Base. *J. Am. Chem. Soc.* **2013**, *135*, 13473−13478.
(42) Zhuang, Z.; Giles, S. A.; Zheng, J.; Jenness, G. R.; Caratzoulas, S.; Vlachos, D. G.; Yan, Y. Nickel Supported on Nitrogen-Doped Carbon Nanotubes as Hydrogen Oxidation Reaction Catalyst in Alkaline Electrolyte. *Nat. Commun.* **2016**, *7*, 10141.
(43) Morozan, A.; Goellner, V.; Nedellec, Y.; Hannauer, J.; Jaouen, F. Effect of the Transition Metal on Metal−Nitrogen−Carbon Catalysts for the Hydrogen Evolution Reaction. *J. Electrochem. Soc.* **2015**, *162*, H719−H726.
(44) Zhang, L.; Chang, Q.; Chen, H.; Shao, M. Recent Advances in Palladium-Based Electrocatalysts for Fuel Cell Reactions and Hydrogen Evolution Reaction. *Nano Energy* **2016**, *29*, 198−219.
(45) Durst, J.; Siebel, A.; Simon, C.; Hasche, F.; Herranz, J.; Gasteiger, H. A. New Insights into the Electrochemical Hydrogen Oxidation and Evolution Reaction Mechanism. *Energy Environ. Sci.* **2014**, *7*, 2255−2260.
(46) Marković, N. M.; Sarraf, S. T.; Gasteiger, H. A.; Ross, P. N., Jr. Hydrogen Electrochemistry on Platinum Low-Index Single-Crystal Surfaces in Alkaline Solution. *J. Chem. Soc., Faraday Trans.* **1996**, *92*, 3719−3725.
(47) Maruyama, J.; Inaba, M.; Katakura, K.; Ogumi, Z.; Takehara, Z. Influence of Nafion® Film on the Kinetics of Anodic Hydrogen Oxidation. *J. Electroanal. Chem.* **1998**, *447*, 201−209.
(48) Chen, S.; Kucernak, A. Electrocatalysis under Conditions of High Mass Transport Rate: Oxygen Reduction on Single Submicrometer-Sized Pt Particles Supported on Carbon. *J. Phys. Chem. B* **2004**, *108*, 3262−3276.
(49) Harrison, J.; Khan, Z. The Oxidation of Hydrogen. *J. Electroanal. Chem. Interfacial Electrochem.* **1971**, *30*, 327−330.


DOI: 10.1021/acscatal.8b00689
*ACS Catal.* 2018, 8, 6665−6690

(50) Vogel, W.; Lundquist, L.; Ross, P.; Stonehart, P. Reaction Pathways and Poisons-II. The Rate Controlling Step for Electrochemical Oxidation of Hydrogen on Pt in Acid and Poisoning of the Reaction by CO. *Electrochim. Acta* **1975**, *20*, 79−93.
(51) Ross, P. N.; Stonehart, P. Correlations between Electrochemical Activity and Heterogeneous Catalysis for Hydrogen Dissociation on Platinum. *J. Res. Inst. Catal., Hokkaido Univ.* **1975**, *22*, 22−41.
(52) Guilminot, E.; Corcella, A.; Chatenet, M.; Maillard, F. Comparing the Thin-Film Rotating Disk Electrode and the Ultramicroelectrode with Cavity Techniques to Study Carbon-Supported Platinum for Proton Exchange Membrane Fuel Cell Applications. *J. Electroanal. Chem.* **2007**, *599*, 111−120.
(53) Tu, W.; Liu, W.; Cha, C.; Wu, B. Study of the Powder/Membrane Interface by Using the Powder Microelectrode Technique I. The Pt-Black/Nafion® Interfaces. *Electrochim. Acta* **1998**, *43*, 3731−3739.
(54) Jiang, J.; Wu, B.; Cha, C.; Zhai, R. Application of SPE composite microelectrodes to the study of the spillover of adsorbed species on electrode surfaces. *J. Electroanal. Chem.* **1998**, *445*, 13−16.
(55) Zalitis, C. M.; Kramer, D.; Kucernak, A. R. Electrocatalytic Performance of Fuel Cell Reactions at Low Catalyst Loading and High Mass Transport. *Phys. Chem. Chem. Phys.* **2013**, *15*, 4329−4340.
(56) LaConti, A. B.; Swette, L. In *Handbook of Fuel Cells: Fundamentals, Technology and Applications*; Vielstich, W., Lamm, A., Gasteiger, H. A., Yokokawa, H., Eds.; John Wiley & Sons: Chichester, U.K., 2010; Vol. *4*, pp 1−17.
(57) Neyerlin, K. C.; Gu, W.; Jorne, J.; Gasteiger, H. A. Study of the Exchange Current Density for the Hydrogen Oxidation and Evolution Reactions. *J. Electrochem. Soc.* **2007**, *154*, B631−B635.
(58) Woodroof, M. D.; Wittkopf, J. A.; Gu, S.; Yan, Y. S. Exchange Current Density of the Hydrogen Oxidation Reaction on Pt/C in Polymer Solid Base Electrolyte. *Electrochem. Commun.* **2015**, *61*, 57−60.
(59) Tafel, J. Über die Polarisation bei kathodischer Wasserstoffentwicklung. *Z. Phys. Chem.* **1905**, *50U*, 641−654.
(60) Tipler, P. A. *Elementary Modern Physics*; Worth Publishers: New York, 1992.
(61) Zheng, J.; Zhuang, Z.; Xu, B.; Yan, Y. Correlating Hydrogen Oxidation/Evolution Reaction Activity with the Minority Weak Hydrogen-Binding Sites on Ir/C Catalysts. *ACS Catal.* **2015**, *5*, 4449−4455.
(62) Bagotzky, V. S.; Osetrova, N. V. Investigations of Hydrogen Ionization on Platinum with the Help of Micro-Electrodes. *J. Electroanal. Chem. Interfacial Electrochem.* **1973**, *43*, 233−249.
(63) Singh, N.; Upham, D. C.; Metiu, H.; McFarland, E. W. Gas-Phase Chemistry to Understand Electrochemical Hydrogen Evolution and Oxidation on Doped Transition Metal Sulfides. *J. Electrochem. Soc.* **2013**, *160*, A1902−A1906.
(64) Conrad, H.; Ertl, G.; Latta, E. E. Adsorption of Hydrogen on Palladium Single Crystal Surfaces. *Surf. Sci.* **1974**, *41*, 435−446.
(65) Choi, C. H.; Kim, M.; Kwon, H. C.; Cho, S. J.; Yun, S.; Kim, H.-T.; Mayrhofer, K. J. J.; Kim, H.; Choi, M. Tuning Selectivity of Electrochemical Reactions by Atomically Dispersed Platinum Catalyst. *Nat. Commun.* **2016**, *7*, 10922.
(66) Christmann, K. Interaction of Hydrogen with Solid Surfaces. *Surf. Sci. Rep.* **1988**, *9*, 1−163.
(67) Paál, Z.; Menon, P. G. *Hydrogen Effects in Catalysis: Fundamentals and Practical Applications*; Marcel Dekker: New York, 1988.
(68) Mitsui, T.; Rose, M. K.; Fomin, E.; Ogletree, D. F.; Salmeron, M. Dissociative Hydrogen Adsorption on Palladium Requires Aggregates of Three or More Vacancies. *Nature* **2003**, *422*, 705−707.
(69) Heyrovsky, J. A Theory of Overpotential. *Recl. des Trav. Chim. des Pays-Bas* **1927**, *46*, 582−585.
(70) Strmcnik, D.; Uchimura, M.; Wang, C.; Subbaraman, R.; Danilovic, N.; van der Vliet, D.; Paulikas, A. P.; Stamenkovic, V. R.; Markovic, N. M. Improving the Hydrogen Oxidation Reaction Rate by Promotion of Hydroxyl Adsorption. *Nat. Chem.* **2013**, *5*, 300−306.
(71) Bakos, I.; Paszternak, A.; Zitoun, D. Pd/Ni Synergestic Activity for Hydrogen Oxidation Reaction in Alkaline Conditions. *Electrochim. Acta* **2015**, *176*, 1074−1082.
(72) Erdey-Grúz, T.; Volmer, M. Zur Theorie der Wasserstoff Überspannung. *Z. Phys. Chem.* **1930**, *150A*, 203−205.
(73) Okamoto, G.; Horiuti, J.; Hirota, K. A Different Application of the Theory, Based on an Assumed Mechanism. *Sci. Pap. Inst. Phys. Chem. Res. Tokyo* **1936**, *29*, 223−227.
(74) Horiuti, J. Hydrogen Intermediates on Catalysts and Electrodes: Part I Fundamental. *J. Res. Inst. Catal., Hokkaido Univ.* **1954**, *3*, 52−107.
(75) Stonehart, P.; Lundquist, J. Platinum Crystallite Size Effects on the Electrocatalytic Oxidation and Deposition of Adsorbed Hydrogen-III. *Electrochim. Acta* **1973**, *18*, 907−911.
(76) Stonehart, P.; Kohlmayr, G. Effect of Poisons on Kinetic Parameters for Platinum Electrocatalyst Sites. *Electrochim. Acta* **1972**, *17*, 369−382.
(77) Bhowmik, T.; Kundu, M. K.; Barman, S. Palladium Nanoparticle-Graphitic Carbon Nitride Porous Synergistic Catalyst for Hydrogen Evolution/Oxidation Reactions over a Broad Range of pH and Correlation of Its Catalytic Activity with Measured Hydrogen Binding Energy. *ACS Catal.* **2016**, *6*, 1929−1941.
(78) Marković, N. M.; Ross, P. N., Jr. Surface Science Studies of Model Fuel Cell Electrocatalysts. *Surf. Sci. Rep.* **2002**, *45*, 117−229.
(79) Nørskov, J. K.; Bligaard, T.; Logadottir, A.; Kitchin, J. R.; Chen, J. G.; Pandelov, S.; Stimming, U. Trends in the Exchange Current for Hydrogen Evolution. *J. Electrochem. Soc.* **2005**, *152*, J23−J26.
(80) Soares, D. M. Hydride Effect on the Kinetics of the Hydrogen Evolution Reaction on Nickel Cathodes in Alkaline Media. *J. Electrochem. Soc.* **1992**, *139*, 98−105.
(81) Floner, D.; Lamy, C.; Leger, J. M. Electrocatalytic Oxidation of Hydrogen on Polycrystal and Single-Crystal Nickel Electrodes. *Surf. Sci.* **1990**, *234*, 87−97.
(82) Vilekar, S. A.; Fishtik, I.; Datta, R. Kinetics of the Hydrogen Electrode Reaction. *J. Electrochem. Soc.* **2010**, *157*, B1040−B1050.
(83) Sheng, W.; Zhuang, Z.; Gao, M.; Zheng, J.; Chen, J. G.; Yan, Y. Correlating Hydrogen Oxidation and Evolution Activity on Platinum at Different pH with Measured Hydrogen Binding Energy. *Nat. Commun.* **2015**, *6*, 5848.
(84) Conway, B. E.; Tilak, B. V. Interfacial Processes Involving Electrocatalytic Evolution and Oxidation of H2, and the Role of Chemisorbed H. *Electrochim. Acta* **2002**, *47*, 3571−3594.
(85) Garcia-Garcia, R.; Ortega-Zarzosa, G.; Rincón, M. E.; Orozco, G. The Hydrogen Evolution Reaction on Rhenium Metallic Electrodes: A Selected Review and New Experimental Evidence. *Electrocatalysis* **2015**, *6*, 263−273.
(86) Garcia-Garcia, R.; Rivera, J. G.; Antaño-Lopez, R.; Castañeda-Olivares, F.; Orozco, G. Impedance Spectra of the Cathodic Hydrogen Evolution Reaction on Polycrystalline Rhenium. *Int. J. Hydrogen Energy* **2016**, *41*, 4660−4669.
(87) Hall, D. S.; Bock, C.; Macdougall, B. R. The Electrochemistry of Metallic Nickel : Oxides, Hydroxides, Hydrides and Alkaline Hydrogen Evolution. *J. Electrochem. Soc.* **2013**, *160*, F235−F243.
(88) Visscher, W.; Barendrecht, E. The Anodic Oxidation of Nickel in Alkaline Solution. *Electrochim. Acta* **1980**, *25*, 651−655.
(89) Albani, O. A.; Gassa, L. M.; Zerbino, J. O.; Vilche, J. R.; Arvia, A. J. Comparative Study of the Passivity and the Breakdown of Passivity of Polycrystalline Iron in Different Alkaline Solutions. *Electrochim. Acta* **1990**, *35*, 1437−1444.
(90) Schrebler Guzmán, R. S.; Vilche, J. R.; Arvía, A. J. The Potentiodynamic Behaviour of Iron in Alkaline Solutions. *Electrochim. Acta* **1979**, *24*, 395−403.
(91) Geana, D.; El Miligy, A. A.; Lorenz, W. J. Electrochemical Behaviour of Iron in Alkaline Sulphate Solutions. *J. Appl. Electrochem.* **1974**, *4*, 337−345.
(92) Couturier, G.; Kirk, D. W.; Hyde, P. J.; Srinivasan, S. Electrocatalysis of the Hydrogen Oxidation and of the Oxygen Reduction Reactions of Pt and Some Alloys in Alkaline Medium. *Electrochim. Acta* **1987**, *32*, 995−1005.


DOI: 10.1021/acscatal.8b00689
*ACS Catal.* 2018, 8, 6665−6690

(93) Jaksic, M.; Johansen, B.; Tunold, R. Electrochemical Behaviour of Rhodium in Alkaline and Acidic Solutions of Heavy and Regular Water. *Int. J. Hydrogen Energy* **1994**, *19*, 35−51.
(94) Tarasevich, M. R.; Davydova, E. S.; Modestov, A. D.; Kazanskii, L. P.; Pu, H. Properties of Anodic $RuNiO_X(OH)_Y$ Catalysts Synthesized on Carbon Supports with Various Dispersion Degree. *Russ. J. Electrochem.* **2012**, *48*, 82−88.
(95) Montero, M. A.; De Chialvo, M. R. G.; Chialvo, A. C. Evaluation of the Kinetic Parameters of the Hydrogen Oxidation Reaction on Nanostructured Iridium Electrodes in Alkaline Solution. *J. Electroanal. Chem.* **2016**, *767*, 153−159.
(96) Morozan, A.; Goellner, V.; Zitolo, A.; Fonda, E.; Donnadieu, B.; Jones, D.; Jaouen, F. Synergy between Molybdenum Nitride and Gold Leading to Platinum-like Activity for Hydrogen Evolution. *Phys. Chem. Chem. Phys.* **2015**, *17*, 4047−4053.
(97) Schmidt, T. J.; Ross, P. N.; Markovic, N. M. Temperature Dependent Surface Electrochemistry on Pt Single Crystals in Alkaline Electrolytes: Part 2. The Hydrogen Evolution/oxidation Reaction. *J. Electroanal. Chem.* **2002**, *524-525*, 252−260.
(98) Schmidt, T. J.; Ross, P. N.; Markovic, N. M. Temperature-Dependent Surface Electrochemistry on Pt Single Crystals in Alkaline Electrolyte: Part 1: CO Oxidation. *J. Phys. Chem. B* **2001**, *105*, 12082−12086.
(99) Schouten, K. J. P.; van der Niet, M. J. T. C.; Koper, M. T. M. Impedance Spectroscopy of H and OH Adsorption on Stepped Single-Crystal Platinum Electrodes in Alkaline and Acidic Media. *Phys. Chem. Chem. Phys.* **2010**, *12*, 15217.
(100) van der Niet, M. J. T. C.; Garcia-Araez, N.; Hernández, J.; Feliu, J. M.; Koper, M. T. M. Water Dissociation on Well-Defined Platinum Surfaces: The Electrochemical Perspective. *Catal. Today* **2013**, *202*, 105−113.
(101) Gisbert, R.; García, G.; Koper, M. T. M. Adsorption of Phosphate Species on Poly-Oriented Pt and Pt(111) Electrodes over a Wide Range of pH. *Electrochim. Acta* **2010**, *55*, 7961−7968.
(102) Nørskov, J. K.; Bligaard, T.; Logadottir, A.; Bahn, S.; Hansen, L. B.; Bollinger, M.; Bengaard, H.; Hammer, B.; Sljivancanin, Z.; Mavrikakis, M.; et al. Universality in Heterogeneous Catalysis. *J. Catal.* **2002**, *209*, 275−278.
(103) Motoo, S.; Furuya, N. Effect of Anions on Hydrogen and Oxygen Adsorption on Iridium Single Cyrstal Surfaces. *J. Electroanal. Chem. Interfacial Electrochem.* **1984**, *181*, 301−305.
(104) Santos, E.; Pinto, L. M. C.; Soldano, G.; Innocente, A. F.; Ângelo, A. C. D.; Schmickler, W. Hydrogen Oxidation on Ordered Intermetallic Phases of Platinum and Tin − A Combined Experimental and Theoretical Study. *Catal. Today* **2013**, *202*, 191−196.
(105) Scofield, M. E.; Zhou, Y.; Yue, S.; Wang, L.; Su, D.; Tong, X.; Vukmirovic, M. B.; Adzic, R. R.; Wong, S. S. Role of Chemical Composition in the Enhanced Catalytic Activity of Pt-Based Alloyed Ultrathin Nanowires for the Hydrogen Oxidation Reaction under Alkaline Conditions. *ACS Catal.* **2016**, *6*, 3895−3908.
(106) Elbert, K.; Hu, J.; Ma, Z.; Zhang, Y.; Chen, G.; An, W.; Liu, P.; Isaacs, H. S.; Adzic, R. R.; Wang, J. X. Elucidating Hydrogen Oxidation/Evolution Kinetics in Base and Acid by Enhanced Activities at the Optimized Pt Shell Thickness on the Ru Core. *ACS Catal.* **2015**, *5*, 6764−6772.
(107) Poltorak, O. M.; Boronin, V. S. Mitohedria as a New Method of Studying Active Centers of Crystalline Catalysts. *Zh. Fiz. Khim. SSSR* **1966**, *40*, 2671−2676.
(108) Marković, N. M.; Grgur, B. N.; Ross, P. N. Temperature-Dependent Hydrogen Electrochemistry on Platinum Low-Index Single-Crystal Surfaces in Acid Solutions. *J. Phys. Chem. B* **1997**, *101*, 5405−5413.
(109) Friebel, D.; Viswanathan, V.; Miller, D. J.; Anniyev, T.; Ogasawara, H.; Larsen, A. H.; O'Grady, C. P.; Nørskov, J. K.; Nilsson, A. Balance of Nanostructure and Bimetallic Interactions in Pt Model Fuel Cell Catalysts: In Situ XAS and DFT Study. *J. Am. Chem. Soc.* **2012**, *134*, 9664−9671.
(110) Zadick, A.; Dubau, L.; Sergent, N.; Berthomé, G.; Chatenet, M. Huge Instability of Pt/C Catalysts in Alkaline Medium. *ACS Catal.* **2015**, *5*, 4819−4824.
(111) Nikkuni, F. R.; Dubau, L.; Ticianelli, E. A.; Chatenet, M. Accelerated Degradation of Pt3Co/C and Pt/C Electrocatalysts Studied by Identical-Location Transmission Electron Microscopy in Polymer Electrolyte Environment. *Appl. Catal., B* **2015**, *176−177*, 486−499.
(112) Henning, S.; Herranz, J.; Gasteiger, H. A. Bulk-Palladium and Palladium-on-Gold Electrocatalysts for the Oxidation of Hydrogen in Alkaline Electrolyte. *J. Electrochem. Soc.* **2015**, *162*, F178−F189.
(113) Martin, M. H.; Lasia, A. Hydrogen Sorption in Pd Monolayers in Alkaline Solution. *Electrochim. Acta* **2009**, *54*, 5292−5299.
(114) Zheng, J.; Zhou, S.; Gu, S.; Xu, B.; Yan, Y. Size-Dependent Hydrogen Oxidation and Evolution Activities on Supported Palladium Nanoparticles in Acid and Base. *J. Electrochem. Soc.* **2016**, *163*, F499−F506.
(115) Zadick, A.; Dubau, L.; Demirci, U. B.; Chatenet, M. Effects of Pd Nanoparticle Size and Solution Reducer Strength on Pd/C Electrocatalyst Stability in Alkaline Electrolyte. *J. Electrochem. Soc.* **2016**, *163*, F781−F787.
(116) Kabir, S.; Zadick, A.; Atanassov, P.; Dubau, L.; Chatenet, M. Stability of Carbon-Supported Palladium Nanoparticles in Alkaline Media: A Case Study of Graphitized and More Amorphous Supports. *Electrochem. Commun.* **2017**, *78*, 33−37.
(117) Ohyama, J.; Sato, T.; Yamamoto, Y.; Arai, S.; Satsuma, A. Size Specifically High Activity of Ru Nanoparticles for Hydrogen Oxidation Reaction in Alkaline Electrolyte. *J. Am. Chem. Soc.* **2013**, *135*, 8016−8021.
(118) Montero, M. A.; Fernández, J. L.; Gennero de Chialvo, M. R.; Chialvo, A. C. Kinetic Study of the Hydrogen Oxidation Reaction on Nanostructured Iridium Electrodes in Acid Solutions. *J. Phys. Chem. C* **2013**, *117*, 25269−25275.
(119) Montero, M. A.; Fernández, J. L.; Gennero De Chialvo, M. R.; Chialvo, A. C. Characterization and Kinetic Study of a Nanostructured Rhodium Electrode for the Hydrogen Oxidation Reaction. *J. Power Sources* **2014**, *254*, 218−223.
(120) Ewe, H.; Justi, E.; Schmitt, A. Untersuchungen Zur Konservierung von Raney-Nickel-Misch-Katalysatoren. *Energy Convers.* **1975**, *14*, 35−41.
(121) Ewe, H.; Justi, E.; Schmitt, A. Struktur Und Eigenschaften von Raney-Nickel-Katalysatoren Mit Zulegierungen Für Alkalische Brennstoffzellen. *Electrochim. Acta* **1974**, *19*, 799−808.
(122) Chatterjee, A. K.; Banerjee, R.; Sharon, M. Enhancement of Hydrogen Oxidation Activity at a Nickel Coated Carbon Beads Electrode by Cobalt and Iron. *J. Power Sources* **2004**, *137*, 216−221.
(123) Mund, K.; Richter, G.; von Sturm, F. Titanium-Containing Raney Nickel Catalyst for Hydrogen Electrodes in Alkaline Fuel Cell Systems. *J. Electrochem. Soc.* **1977**, *124*, 1−6.
(124) Lee, H.-K.; Jung, E.-E.; Lee, J.-S. Enhancement of Catalytic Activity of Raney Nickel by Cobalt Addition. *Mater. Chem. Phys.* **1998**, *55*, 89−93.
(125) Kenjo, T. Doping Effects of Transition Metals on the Polarization Characteristics in Raney Nickel Hydrogen Electrodes. *Electrochim. Acta* **1988**, *33*, 41−46.
(126) Jenseit, W.; Khalil, A.; Wendt, H. Material Properties and Processing in the Production of Fuel Cell Components: I. Hydrogen Anodes from Raney Nickel for Lightweight Alkaline Fuel Cells. *J. Appl. Electrochem.* **1990**, *20*, 893−900.
(127) Raj, I. A.; Vasu, K. I. Transition Metal-Based Hydrogen Electrodes in Alkaline Solution - Electrocatalysis on Nickel Based Binary Alloy Coatings. *J. Appl. Electrochem.* **1990**, *20*, 32−38.
(128) Al-Saleh, M. A.; Gultekin, S.; Al-Zakri, A. S.; Khan, A. A. A. Steady State Performance of Copper Impregnated Ni/PTFE Diffusion Electrode in Alkaline Fuel Cell. *Int. J. Hydrogen Energy* **1996**, *21*, 657−661.
(129) Sleem-Ur-Rahman; Al-Saleh, M. A.; Al-Zakri, A. S.; Gultekin, S. Preparation of Raney-Ni Gas Diffusion Electrode by Filtration Method for Alkaline Fuel Cells. *J. Appl. Electrochem.* **1997**, *27*, 215−220.


DOI: 10.1021/acscatal.8b00689
*ACS Catal.* 2018, 8, 6665−6690

(130) Al-Saleh, M. A.; Sleem-Ur-Rahman; Kareemuddin, S. M. M. J.; Al-Zakri, A. S. Novel Methods of Stabilization of Raney-Nickel Catalyst for Fuel-Cell Electrodes. *J. Power Sources* **1998**, *72*, 159−164.
(131) Kiros, Y.; Schwartz, S. Long-Term Hydrogen Oxidation Catalysts in Alkaline Fuel Cells. *J. Power Sources* **2000**, *87*, 101−105.
(132) Kiros, Y.; Majari, M.; Nissinen, T. A. A. Effect and Characterization of Dopants to Raney Nickel for Hydrogen Oxidation. *J. Alloys Compd.* **2003**, *360*, 279−285.
(133) Linnekoski, J. A.; Krause, A. O. I.; Keskinen, J.; Lamminen, J.; Anttila, T. Processing of Raney-Nickel Catalysts for Alkaline Fuel Cell Applications. *J. Fuel Cell Sci. Technol.* **2007**, *4*, 45−48.
(134) Sheng, W.; Bivens, A. P.; Myint, M.; Zhuang, Z.; Forest, R. V.; Fang, Q.; Chen, J. G.; Yan, Y. Non-Precious Metal Electrocatalysts with High Activity for Hydrogen Oxidation Reaction in Alkaline Electrolytes. *Energy Environ. Sci.* **2014**, *7*, 1719−1724.
(135) Kenjo, T. Chromium-Doped Raney Nickel Catalyst for Hydrogen Electrodes in Alkaline Fuel Cells. *J. Electrochem. Soc.* **1985**, *132*, 383.
(136) Tanaka, H.; Kaneki, N.; Hara, H.; Shimada, K.; Takeuchi, T. La−Ni System Porous Anode in an Alkaline Fuel Cell. *Can. J. Chem. Eng.* **1986**, *64*, 267−271.
(137) Al-Saleh, M. Steady State Performance of Copper Impregnated Ni/PTFE Gas Diffusion Electrode in Alkaline Fuel Cell. *Int. J. Hydrogen Energy* **1996**, *21*, 657−661.
(138) Fan, C.; Piron, D.; Rojas, M. Polarization of Cobalt-Molybdenum and Nickel-Molybdenum Hydrogen Electrodes for Alkaline Fuel Cells. *Int. J. Hydrogen Energy* **1994**, *19*, 29−33.
(139) Schulze, M.; Gülzow, E.; Steinhilber, G. Activation of Nickel-Anodes for Alkaline Fuel Cells. *Appl. Surf. Sci.* **2001**, *179*, 251−256.
(140) Dekel, D.; Gottesfeld, S. Anode Electro-Catalysts for Alkaline Membrane Fuel Cells. WO 2013184269 A2, 2013.
(141) Gottesfeld, S.; Dekel, D. Anode Electro-Catalysts for Alkaline Membrane Fuel Cells. US20130295485 A1, 2013.
(142) Dekel, D.; Gottesfeld, S. Anode Electro-Catalysts for Alkaline Membrane Fuel Cells. CA 2872633 A1, 2013.
(143) Celiker, H.; Al-Saleh, M. A.; Gultekin, S.; Al-Zakri, A. S. A Mathematical Model for the Performance of Raney Metal Gas Diffusion Electrodes. *J. Electrochem. Soc.* **1991**, *138*, 1671−1681.
(144) Ewe, H.; Justi, E. W.; Selbach, H.-J. Improvement of the Catalytic Properties of Ti-Doted Raney-Nickel for $H_2$-Anodes of Alkalione Fuel Cells by Ni(OH)2-Surface Coating. *Energy Convers. Manage.* **1983**, *23*, 245−250.
(145) Mohsenzadeh, A.; Bolton, K.; Richards, T. DFT Study of the Adsorption and Dissociation of Water on Ni(111), Ni(110) and Ni(100) Surfaces. *Surf. Sci.* **2014**, *627*, 1−10.
(146) Mohsenzadeh, A.; Richards, T.; Bolton, K. DFT Study of the Water Gas Shift Reaction on Ni(111), Ni(100) and Ni(110) Surfaces. *Surf. Sci.* **2016**, *644*, 53−63.
(147) Angely, L.; Bronoel, G.; Peslerbe, G. Relation between Nickel Crystalline Structures and Their Electrocatalytic Properties. *J. Electroanal. Chem. Interfacial Electrochem.* **1979**, *96*, 191−201.
(148) Zadick, A.; Dubau, L.; Artyushkova, K.; Serov, A.; Atanassov, P.; Chatenet, M. Nickel-Based Electrocatalysts for Ammonia Borane Oxidation: Enabling Materials for Carbon-Free-Fuel Direct Liquid Alkaline Fuel Cell Technology. *Nano Energy* **2017**, *37*, 248−259.
(149) Kattel, S.; Duan, Z.; Wang, G. Density Functional Theory Study of an Oxygen Reduction Reaction on a $Pt_3Ti$ Alloy Electrocatalyst. *J. Phys. Chem. C* **2013**, *117*, 7107−7113.
(150) Greeley, J.; Stephens, I. E. L.; Bondarenko, A. S.; Johansson, T. P.; Hansen, H. A.; Jaramillo, T. F.; Rossmeisl, J.; Chorkendorff, I.; Nørskov, J. K. Alloys of Platinum and Early Transition Metals as Oxygen Reduction Electrocatalysts. *Nat. Chem.* **2009**, *1*, 552−556.
(151) Han, B. C.; Miranda, C. R.; Ceder, G. Effect of Particle Size and Surface Structure on Adsorption of O and OH on Platinum Nanoparticles: A First-Principles Study. *Phys. Rev. B: Condens. Matter Mater. Phys.* **2008**, *77*, 075410.
(152) Lin, C. X.; Sekachev, M.; Hu, Z.; Dareing, D. A Computational DFT Analysis of OH Chemisorption on Catalytic Pt(111) Nanoparticles. *J. Nanopart. Res.* **2010**, *12*, 865−876.
(153) Mazher, J.; Al-Odail, F. A. Hydrogen Oxidation Reaction on Pd(111) Electrode in Alkaline Media: Ab-Initio DFT Study of OH Effects. *Comput. Theor. Chem.* **2015**, *1063*, 63−69.
(154) Quaino, P.; Arce, M. D.; Santos, E.; Schmickler, W. A First Principles Study of the Hydrogen Reaction in Alkaline Media: OH Effect. *Int. J. Hydrogen Energy* **2012**, *37*, 14796−14800.
(155) Balbuena, P. B.; Altomare, D.; Vadlamani, N.; Bingi, S.; Agapito, L. A.; Seminario, J. M. Adsorption of O, OH, and $H_2O$ on Pt-Based Bimetallic Clusters Alloyed with Co, Cr, and Ni. *J. Phys. Chem. A* **2004**, *108*, 6378−6384.
(156) Michaelides, A.; Hu, P. Density Functional Theory Study of Hydroxyl and the Intermediate in the Water Formation Reaction on Pt. *J. Chem. Phys.* **2001**, *114*, 513−519.
(157) Gómez-Marín, A. M.; Hernández-Ortiz, J. P. Langmuir-Hinshelwood Mechanism Including Lateral Interactions and Species Diffusion for CO Electro-Oxidation on Metallic Surfaces. *J. Phys. Chem. C* **2014**, *118*, 2475−2486.
(158) Climent, V.; Attard, G. A.; Feliu, J. M. Potential of Zero Charge of Platinum Stepped Surfaces: A Combined Approach of CO Charge Displacement and $N_2O$ Reduction. *J. Electroanal. Chem.* **2002**, *532*, 67−74.
(159) Bensalem, A.; Bozon-Verduraz, F.; Perrichon, V. Palladium-Ceria Catalysts: Reversibility of Hydrogen Chemisorption and Redox Phenomena. *J. Chem. Soc., Faraday Trans.* **1995**, *91*, 2185.
(160) Ramaswamy, N.; Ghoshal, S.; Bates, M. K.; Jia, Q.; Li, J.; Mukerjee, S. Hydrogen Oxidation Reaction in Alkaline Media: Relationship between Electrocatalysis and Electrochemical Double-Layer Structure. *Nano Energy* **2017**, *41*, 765−771.
(161) Gottesfeld, S.; Dekel, D. R.; Page, M.; Bae, C.; Yan, Y.; Zelenay, P.; Kim, Y. S. Anion Exchange Membrane Fuel Cells: Current Status and Remaining Challenges. *J. Power Sources* **2018**, *375*, 170−184.
(162) Wagner, N.; Schulze, M.; Gülzow, E. Long Term Investigations of Silver Cathodes for Alkaline Fuel Cells. *J. Power Sources* **2004**, *127*, 264−272.
(163) Gülzow, E.; Schulze, M.; Steinhilber, G. Investigation of the Degradation of Different Nickel Anode Types for Alkaline Fuel Cells (AFCs). *J. Power Sources* **2002**, *106*, 126−135.
(164) McLean, G. F.; Niet, T.; Prince-Richard, S.; Djilali, N. An Assessment of Alkaline Fuel Cell Technology. *Int. J. Hydrogen Energy* **2002**, *27*, 507−526.
(165) Villarrubia, C. W. N.; Serov, A.; Dumont, J. H.; Atanassov, P.; Kim, Y. S. Investigating Non-Precious Metal Catalyst−Electrolyte Interface in Anodes for Alkaline Fuel Cells. *Meet. Abstr.—Electrochem. Soc.* **2017**, *232*, 1621.
(166) Yim, S.-D.; Chung, H. T.; Chlistunoff, J.; Kim, D.-S.; Fujimoto, C.; Yang, T.-H.; Kim, Y. S. A Microelectrode Study of Interfacial Reactions at the Platinum-Alkaline Polymer Interface. *J. Electrochem. Soc.* **2015**, *162*, F499−F506.
(167) Chung, H. T.; Martinez, U.; Matanovic, I.; Kim, Y. S. Cation-Hydroxide-Water Coadsorption Inhibits the Alkaline Hydrogen Oxidation Reaction. *J. Phys. Chem. Lett.* **2016**, *7*, 4464−4469.
(168) Chung, H. T.; Choe, Y.-K.; Martinez, U.; Dumont, J. H.; Mohanty, A.; Bae, C.; Matanovic, I.; Kim, Y. S. Effect of Organic Cations on Hydrogen Oxidation Reaction of Carbon Supported Platinum. *J. Electrochem. Soc.* **2016**, *163*, F1503−F1509.
(169) Matanovic, I.; Chung, H. T.; Kim, Y. S. Benzene Adsorption: A Significant Inhibitor for the Hydrogen Oxidation Reaction in Alkaline Conditions. *J. Phys. Chem. Lett.* **2017**, *8*, 4918−4924.


DOI: 10.1021/acscatal.8b00689
*ACS Catal.* 2018, 8, 6665−6690